Two-Dimensional Exact Analytical Method for Steady-State Heat Transfer Prediction in Rotating Electrical Machines

Kamel Boughrara[1], Frédéric Dubas[2], Rachid Ibtiouen[1]

[1]Ecole Nationale Polytechnique (LRE-ENP), Rue des Frères Oudek, Hassan Badi, B.P. 182, El-Harrach, 16200, Alger, Algérie
[2]Département ENERGIE, FEMTO-ST, CNRS, Univ. Bourgogne Franche-Comté, F90000 Belfort, France

Actually, the heat transfer prediction and temperature distribution in electrical machines are realized by using finite-element method (Fem) and/or thermal equivalent circuit (TEC). The analytical resolution of partial differential equations (PDEs) representing the temperature distribution in electrical machines doesn't exist. In this paper, a two-dimensional (2-D) exact analytical calculation of steady-state temperature distribution in rotating electrical machines by solving the heat equation in homogenous and non-homogenous regions by using the Fourier's series and the separation of variables method is presented. It is based on the new subdomain technique where the solution depends on both directions (*r*, *θ*) and able to model the different materials of the machine with different thermal conductivities. The heat sources are volumique power losses due to hysteresis, eddy-current and Joule losses in all the regions of machine. A simplified method is used to determine the power losses in permanent-magnet (PM) motors. The main studied problem is conductive with conductive interface conditions (ICs). Although, convective heat transfer in the air-gap is also investigated. The boundary conditions (BCs) considered for solving the conduction problem is a convective heat transfer between the machine and external air and at the rotor internal air. The semi-analytical results are in very good agreement with those obtained by Fem, considering both amplitude and waveform.

***Index Terms*—air-gap convection, conductive heat transfer, exact subdomain technique, numerical, thermal model, two-dimensional.**

I. Introduction

Accurate thermal models of electrical machines are often necessary for their design, analysis and system insulation optimization. Knowing the temperature and heat flux distribution created by the power losses is very important for the insulation determination and the process to apply it. Many researchers have studied the temperature distribution in electrical machines by using Fem and/or TEC (i.e., thermal resistances network, thermal lumped circuit,…) **[1]**-**[4]**. This later method is considered as an analytical method. It is based on the resolution of a system of equations representing the different nodes of the network. However, in our best knowledge, there is not any analytical calculation of heat transfer by using the formal resolution of heat PDEs in electrical machines. There is only one reference **[5]** where the author has calculated analytically the steady-state temperature in radial and axial directions (*r*, *z*) inside the magnet (one region) of a PM machine.

The most used method in thermal modeling of electrical machines is TEC which is able to predict the temperature distribution in steady-state and/or transient. It is based on the representation of the machine materials by different thermal resistances representing the thermal conduction, convection and radiation. This method is fast and can be used to determine the necessary insulation characteristics and normal temperature functioning of the machine **[6]**-**[8]**. Although, there are many different lumped circuits that can be adopted for representing the heat transfer in an electrical machine. The thermal designers chose generally a TEC with low number of nodes and thermal resistances especially in transient calculation. The numerical methods are also frequently used to analyze the machine's temperatures and heat transfer due to power losses (i.e., hysteresis losses, eddy-current losses and Joule losses). The thermal calculation by using Fem can be done alone using power losses as heat sources or coupled directly to electromagnetic analysis **[3]** and **[9]**-**[11]**. The Fem and computational fluid dynamics (CFD) take into account the variation of materials conductivities with temperature and permit to model convective problems accurately **[12]**-**[13]**. Recently, there are some references that used a hybrid method. The stator and rotor TEC is coupled to an exact analytical solution only in the air-gap **[14]**-**[15]**.

In this paper, we present a new 2-D exact analytical prediction of steady-state temperature and heat flux in rotating electrical machines considering a conductive heat transfer inside the machine and air-gap and convective heat transfer outside the machine and inside rotor. It is based on the 2-D exact subdomain technique in polar coordinates developed by Dubas and Boughrara (2017) **[16]** and applied to radial-flux electrical machines for electromagnetic performances calculation **[17]**. In this paper, this novel scientific contribution allows to take into account the different materials conductivities (i.e., stator/rotor iron, air, air-gap, PM, slots coils, cage bars). Of course, the conventional subdomain technique used by many authors in electromagnetic performances prediction cannot be applied to thermal modeling even if the heat equations in the different regions of the machine are similar to magnetic differential equations. The conventional subdomain technique considers the ferromagnetic iron having infinity permeability **[18]**-**[21]** and cannot take into account the different thermal conductivities of the machine. This is why at this time there is not any prediction of heat transfer in electrical machines using the subdomain technique. In **[17]**, the authors confirmed also that the approach applied to electrical machines is less time consuming (12 sec) in comparison with Fem (20 sec). The developed analytical method is used to determine heat transfer in surface-mounted PM machine (SPM), inset PM machine (IPM), induction machine (IM) with cage rotor, and spoke-type PM machine (Spoke). Moreover, it is valid for most electrical machines.

The heat transfer by convection in the air-gap of IPM is also investigated by using the developed analytical method. However, it cannot be validated with the used Fem code **[22]** and necessitate a Fem with CFD **[23]-[25]**. This is why we have limited the investigation of air-gap convection to IPM only. The next step in the analytical thermal modeling of rotating machines would be the introduction of the conductivity variation with the temperature. This variation is similar to the *B(H)* curve in the iron for the saturation effect and can be introduced in the same way **[26]**. To determine the heat sources, a simple method is used to determine power losses for studied SPM and IPM **[27]**. Heat sources of IM and Spoke machines are considered similar to those of IPM.

II. Studied Machines and Analytical Temperature Calculation

A. *Problem Description, Assumptions and PDEs*

The main heat transfer studied in this paper is conductive with volumique power sources representing the power losses in each region. Heat PDEs are the Laplace's equation in the air-gap and the Poisson's equations in the other regions. The model is adopted with the following assumptions:

- The materials of the machines are considered isotropic having constant thermal conductivities without any variation with temperature;
- The stator and rotor slots have radial sides;
- The heat sources are uniform and constant in each region (or subdomain);
- The radiation outside stator and inside the rotor is ignored;
- The interfaces between regions are considered perfect.

Four electrical machines have been studied in this paper [see **Fig. 1**], viz., i) a surface-mounted PM machine, ii) an inset PM machine, iii) an induction machine with cage rotor, and iv) a spoke-type PM machine. The analyzed IM has 6 stator slots and 4 bars [see **Fig. 1(c)**].

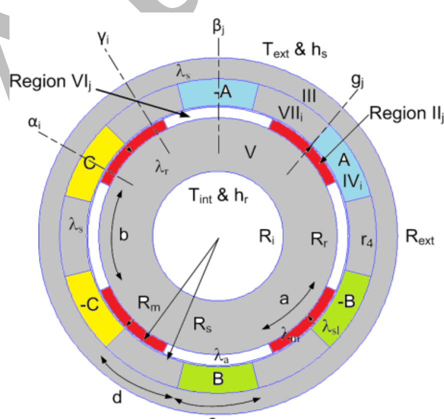

(a) Surface-mounted PM machine (SPM).

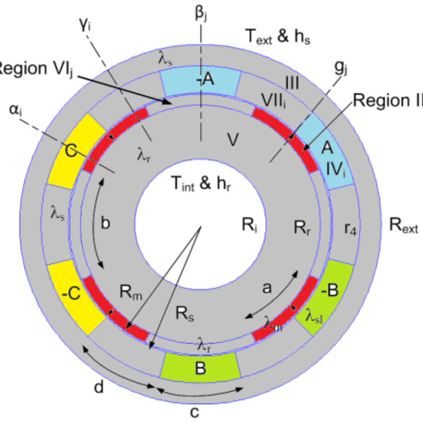

(b) Inset PM machine (IPM).

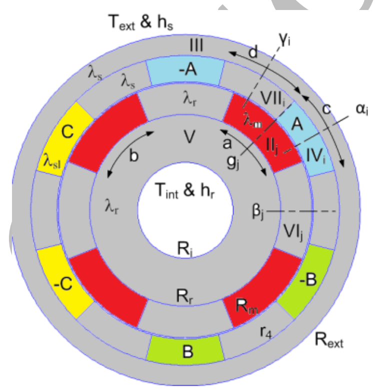

(c) Induction machine (IM).

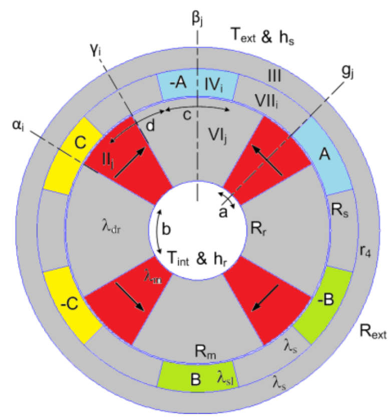

(d) Spoke-type PM machine (Spoke).

Fig. 1: Studied machines.

The machines are subdivided by 7 regions. Region I represents the air-gap, Region IIj the PMs in the SPM, IPM or Spoke and cage bars in the IM, Region III the stator yoke, Region IVi the stator slots, Region V the rotor yoke, Region VIj the air between PMs in the SPM and rotor teeth in the IPM, IM and Spoke, and Region VIIi the stator teeth. It is interesting to note that Region V does not exist in Spoke machine.

In steady-state, the PDEs representing the temperature distribution in each region are given

- in Region I by

$$\lambda_e \cdot \Delta TI(r,\theta) = 0 \qquad (1)$$

where λ_e is the air-gap thermal conductivity (in W/mK).

- in Regions IIj by

$$\Delta TII_j\left(r,\theta\right) = -\frac{Pm_j}{\lambda_m} \qquad (2)$$

where λ_m is the PMs or cage bars thermal conductivity, and Pm_j the power loss density of the j^{th} Region II (in W/m^3).

- in Region III by

$$\Delta TIII\left(r,\theta\right) = -\frac{p_s}{\lambda_s} \qquad (3)$$

where λ_s is the stator yoke thermal conductivity, and p_s the power loss density in the stator iron. This power loss is considered uniform and constant in the whole stator iron.

- in Regions IVi by

$$\Delta TIV_i\left(r,\theta\right) = -\frac{Psl_i}{\lambda_{sl}} \qquad (4)$$

where λ_{sl} is the stator slots thermal conductivity, and Psl_i the Joule losses considered constant in each stator slot.

- in Region V by

$$\Delta TV\left(r,\theta\right) = -\frac{p_r}{\lambda_r} \qquad (5)$$

where λ_r is the rotor yoke thermal conductivity, and p_r the power loss density in the rotor iron.

- in Regions VIj by

$$\Delta TVI_j\left(r,\theta\right) = -\frac{Pdr_j}{\lambda_a} \qquad (6)$$

where λ_a is the air between PMs or rotor teeth thermal conductivity, and Pdr_j the power loss density of the j^{th} Region VI. This power loss is null in the case of the SPM where the region represents the air space between PMs.

- in Regions VIIi by

$$\Delta TVII_i\left(r,\theta\right) = -\frac{Pd_i}{\lambda_d} \qquad (7)$$

where λ_d is the stator teeth thermal conductivity, and Pd_i the power loss density in the stator teeth.

It is noticed that $\lambda_d = \lambda_{ds} = \lambda_s$, $\lambda_a = \lambda_{dr}$ and $\lambda_a = \lambda_{dr} = \lambda_r$ for ferromagnetic material.

Using $\boldsymbol{q} = -\lambda \cdot \nabla \boldsymbol{T}$, the heat flux density components (in W/m^2) in polar coordinates are defined as

$$q_r = -\lambda \frac{\partial T\left(r,\theta\right)}{\partial r} \qquad (8)$$

$$q_\theta = -\frac{\lambda}{r}\frac{\partial T\left(r,\theta\right)}{\partial \theta} \qquad (9)$$

where λ is the thermal conductivity.

B. Temperature Solution in each Subdomain

The steady-state heat transfer in the four machines is studied by using the 2-D exact subdomain technique

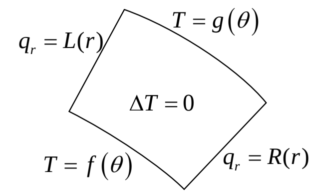

(a) Non-homogenous boundary conditions (BCs).

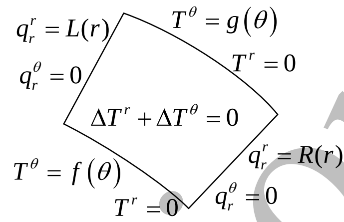

(b) Principle of superposition.

Fig. 2: Region with non-homogenous BCs.

developed recently in **[16]-[17]** with non-homogenous BCs. The subdomains connection is performed directly in both directions (i.e., *r*- and θ-edges ICs) considering the different conductivities of machines. The general solutions of Laplace's and Poisson's equations in non-homogenous BCs [see **Fig. 2(a)**] are deduced by applying the principle of superposition [see **Fig. 2(b)**] and by using the Fourier's series as well as the separation of variables method.

The solution of Laplace's equation **(1)** in the air-gap, where the BCs are homogenous, is given by well-known general form in 2π periodic subdomain:

$$\begin{aligned} TI(r,\theta) &= A1_0 + A2_0 \ln\left(r\right) \\ &\cdots + \sum_{n=1}^{nn}\left(A1_n\left(\frac{r}{R_s}\right)^n + A2_n\left(\frac{r}{R_m}\right)^{-n}\right)\sin\left(n\theta\right) \\ &\cdots + \sum_{n=1}^{nn}\left(A3_n\left(\frac{r}{R_s}\right)^n + A4_n\left(\frac{r}{R_m}\right)^{-n}\right)\cos\left(n\theta\right) \end{aligned} \qquad (10)$$

where R_s and R_m are respectively the external and internal radius of the air gap region. *nn* is the number of harmonics in the air gap, stator yoke and the rotor.

The solution of Poisson's equation **(2)** in Region IIj, where the BCs are non-homogenous, is given by

$$\begin{aligned} TII_j(r,\theta) &= B1_{j,0} + B2_{j,0}\ln\left(r\right) - \frac{Pm_j}{4\lambda_m}r^2 \\ &\cdots + \sum_{m=1}^{mm}\left(B1_{j,m}\left(\frac{r}{R_m}\right)^{fra_m} + B2_{j,m}\left(\frac{r}{R_r}\right)^{-fra_m}\right)\cos\left(fra_m\left(\theta - \theta a1_j\right)\right) \\ &\cdots + \sum_{k=1}^{kk}\left(\begin{array}{l} B3_{j,k}\dfrac{sh\left(fr_k\left(\theta - \theta a1_j\right)\right)}{sh\left(fr_k a\right)} \\ \cdots + B4_{j,k}\dfrac{sh\left(fr_k\left(\theta - \theta a2_j\right)\right)}{sh\left(fr_k a\right)} \end{array}\right)\sin\left(fr_k \ln\left(\frac{r}{R_r}\right)\right) \end{aligned} \qquad (11)$$

where $fr_k = \dfrac{k\pi}{gg}$; $gg = \ln\left(\dfrac{R_m}{R_r}\right)$; $fra_m = \dfrac{m\pi}{a}$; $\theta a1_j = g_j - \dfrac{a}{2}$;

$\theta a2_j = g_j + \frac{a}{2}$; R_r, a and g_j are respectively the internal radius, the opening width and angle of symmetry axis of PM; *kk* and *mm* are the number of harmonics in the PM region.

The stator yoke represented by Region III has homogenous BCs and the solution of **(3)** is

$$
\begin{aligned}
TIII(r,\theta) &= A6_0 + A5_0 \ln(r) - \frac{p_s}{4\lambda_s} r^2 \\
&\cdots + \sum_{n=1}^{nn} \left(A5_n \left(\frac{r}{R_{ext}} \right)^{n} + A6_n \left(\frac{r}{R_{ext}} \right)^{-n} \right) \cos(n\theta) \\
&\cdots + \sum_{n=1}^{nn} \left(A7_n \left(\frac{r}{R_{ext}} \right)^{n} + A8_n \left(\frac{r}{R_{ext}} \right)^{-n} \right) \sin(n\theta)
\end{aligned} \tag{12}
$$

where R_{ext} is the external radius of the machine.

The Q_s stator slots represented by Region IVi with non-homogenous BCs, the solution of **(4)** is given by

$$
\begin{aligned}
TIV_i(r,\theta) &= C1_{i,0} + C2_{i,0} \ln(r) - \frac{Psl_i}{4\lambda_{sl}} r^2 \\
&\cdots + \sum_{m1=1}^{mm1} \left(C1_{i,m1} \left(\frac{r}{r_4} \right)^{fsc_{m1}} + C2_{i,m1} \left(\frac{r}{R_s} \right)^{-fsc_{m1}} \right) \cos\left(fsc_{m1} (\theta - \theta c1_i) \right) \\
&\cdots + \sum_{k1=1}^{kk1} \left(C3_{i,k1} \frac{sh\left(fs_{k1} (\theta - \theta c1_i) \right)}{sh\left(fs_{k1} c \right)} \cdots + C4_{i,k1} \frac{sh\left(fs_{k1} (\theta - \theta c2_i) \right)}{sh\left(fs_{k1} c \right)} \right) \sin\left(fs_{k1} \ln\left(\frac{r}{R_s} \right) \right)
\end{aligned} \tag{13}
$$

where $fs_{k1} = \frac{k1\pi}{ff}$; $ff = \ln\left(\frac{r_4}{R_s}\right)$; $fsc_{m1} = \frac{m1\pi}{c}$; $\theta c1_i = \alpha_i - \frac{c}{2}$; $\theta c2_i = \alpha_i + \frac{c}{2}$; r_4, c and α_i are respectively the external radius of stator slot, the slot opening width and the angle of axis symmetry of slot; *kk1* and *mm1* are the number of harmonics in the stator slot region.

The rotor yoke represented by Region V has homogenous BCs and the solution of **(5)** is

$$
\begin{aligned}
TV(r,\theta) &= A10_0 + A9_0 \ln(r) - \frac{p_r}{4\lambda_r} r^2 \\
&\cdots + \sum_{n=1}^{nn} \left(A9_n \left(\frac{r}{R_i} \right)^{n} + A10_n \left(\frac{r}{R_i} \right)^{-n} \right) \cos(n\theta) \\
&\cdots + \sum_{n=1}^{nn} \left(A11_n \left(\frac{r}{R_i} \right)^{n} + A12_n \left(\frac{r}{R_i} \right)^{-n} \right) \sin(n\theta)
\end{aligned} \tag{14}
$$

where R_i is the radius of rotor shaft.

In Region VIj with non-homogenous BCs, the solution of **(6)** is given by

$$
\begin{aligned}
TVI_j(r,\theta) &= B6_{j,0} + B5_{j,0} \ln(r) - \frac{Pdr_j}{4\lambda_a} r^2 \\
&\cdots + \sum_{m=1}^{mm} \left(B5_{j,m} \left(\frac{r}{R_m} \right)^{frb_m} + B6_{j,m} \left(\frac{r}{R_r} \right)^{-frb_m} \right) \cos\left(frb_m (\theta - \theta b1_j) \right) \\
&\cdots + \sum_{k=1}^{kk} \left(\frac{B7_{j,k} sh\left(fr_k (\theta - \theta b1_j) \right)}{sh(fr_k b)} \cdots + \frac{B8_{j,k} sh\left(fr_k (\theta - \theta b2_j) \right)}{sh(fr_k b)} \right) \sin\left(fr_k \ln\left(\frac{r}{R_r} \right) \right)
\end{aligned} \tag{15}
$$

where $frb_m = \frac{m\pi}{b}$; $\theta b1_j = \beta_j - \frac{b}{2}$; $\theta b2_j = \beta_j + \frac{b}{2}$; b and β_j are respectively the rotor tooth opening width and the angle of symmetry axis of rotor tooth.

In region VIIi representing the stator teeth with Pds_i power losses, we have

$$
\begin{aligned}
TVII_i(r,\theta) &= C5_{i,0} + C6_{i,0} \ln(r) - \frac{Pds_i}{4\lambda_{ds}} r^2 \\
&\cdots + \sum_{m1=1}^{mm1} \left(C5_{i,m1} \left(\frac{r}{r_4} \right)^{fsd_{m1}} + C6_{i,m1} \left(\frac{r}{R_s} \right)^{-fsd_{m1}} \right) \cos\left(fsd_{m1} (\theta - \theta d1_i) \right) \\
&\cdots + \sum_{k1=1}^{kk1} \left(C7_{i,k1} \frac{sh\left(fs_{k1} (\theta - \theta d1_i) \right)}{sh\left(fs_{k1} d \right)} \cdots + C8_{i,k1} \frac{sh\left(fs_{k1} (\theta - \theta d2_i) \right)}{sh\left(fs_{k1} d \right)} \right) \sin\left(fs_{k1} \ln\left(\frac{r}{R_s} \right) \right)
\end{aligned} \tag{16}
$$

where $fs_{k1} = \frac{k1\pi}{ff}$; $ff = \ln\left(\frac{r_4}{R_s}\right)$; $fsd_{m1} = \frac{m1\pi}{d}$; $\theta d1_i = \gamma_i - \frac{d}{2}$; $\theta d2_i = \gamma_i + \frac{d}{2}$; d and γ_i are respectively the stator tooth opening width and the angle of symmetry axis of stator tooth.

C. Interface Conditions in the θ- and r-Directions

To determine the unknown coefficients of temperature in each subdomain, there are 18 ICs, viz., 14 ICs are in the *θ*-direction and 4 ICs in the *r*-direction.

When considering heat transfer inside the machine by conduction and outside the machine by convection, the ICs are given as follow:

- in the *θ*-direction

$$
qV_r(R_i,\theta) = -h_r\left(TV(R_i,\theta) - T_{\text{int}} \right) \tag{17}
$$

where T_{int} and h_r are respectively the temperature and the coefficient of convection of air in the rotor shaft.

$$
TV(R_r,\theta) = TII_j(R_r,\theta) \tag{18}
$$

$$
TV(R_r,\theta) = TVI_j(R_r,\theta) \tag{19}
$$

$$
qV_r(R_r,\theta) = \begin{cases} qII_{r,j}(R_r,\theta) & \text{for } \theta \in \left[g_j + \frac{a}{2}; g_j - \frac{a}{2} \right] \\ qVI_{r,j}(R_r,\theta) & \text{for } \theta \in \left[\beta_j + \frac{b}{2}; \beta_j - \frac{b}{2} \right] \end{cases} \tag{20}
$$

$$
TI(R_m,\theta) = TII_j(R_m,\theta) \tag{21}
$$

$$
TI(R_m,\theta) = TVI_j(R_m,\theta) \tag{22}
$$

$$qI_r\left(R_m,\theta\right)=\begin{cases} qII_{r,j}\left(R_m,\theta\right) & \text{for } \theta\in\left[g_j+\dfrac{a}{2};g_j-\dfrac{a}{2}\right] \\ qVI_{r,j}\left(R_m,\theta\right) & \text{for } \theta\in\left[\beta_j+\dfrac{b}{2};\beta_j-\dfrac{b}{2}\right] \end{cases} \quad (23)$$

$$TI\left(R_s,\theta\right)=TIV_i\left(R_s,\theta\right) \quad (24)$$

$$TI\left(R_s,\theta\right)=TVII_i\left(R_s,\theta\right) \quad (25)$$

$$qI_r\left(R_s,\theta\right)=\begin{cases} qIV_{r,i}\left(R_s,\theta\right) & \text{for } \theta\in\left[\alpha_i+\dfrac{c}{2};\alpha_i-\dfrac{c}{2}\right] \\ qVII_{r,i}\left(R_s,\theta\right) & \text{for } \theta\in\left[\gamma_i+\dfrac{d}{2};\gamma_i-\dfrac{d}{2}\right] \end{cases} \quad (26)$$

$$TIII\left(r_4,\theta\right)=TIV_i\left(r_4,\theta\right) \quad (27)$$

$$TIII\left(r_4,\theta\right)=TVII_i\left(r_4,\theta\right) \quad (28)$$

$$qIII_r\left(r_4,\theta\right)=\begin{cases} qIV_{r,i}\left(r_4,\theta\right) & \text{for } \theta\in\left[\alpha_i+\dfrac{c}{2};\alpha_i-\dfrac{c}{2}\right] \\ qVII_{r,i}\left(r_4,\theta\right) & \text{for } \theta\in\left[\gamma_i+\dfrac{d}{2};\gamma_i-\dfrac{d}{2}\right] \end{cases} \quad (29)$$

$$qIII_r\left(R_{ext},\theta\right)=h_s\left(TIII\left(R_{ext},\theta\right)-T_{ext}\right) \quad (30)$$

where T_{ext} and h_s are respectively the temperature and the coefficient of convection of ambient air of the machine.

- in the *r*-direction

$$qII_{\theta,j}\left(r,g_j+\frac{a}{2}\right)=qVI_{\theta,j}\left(r,\beta_j-\frac{b}{2}\right) \quad (31a)$$

$$qII_{\theta,j}\left(r,g_j-\frac{a}{2}\right)=qVI_{\theta,j}\left(r,\beta_j+\frac{b}{2}\right) \quad (31b)$$

$$TII_j\left(r,g_j+\frac{a}{2}\right)=TVI_j\left(r,\beta_j-\frac{b}{2}\right) \quad (32a)$$

$$TII_j\left(r,g_j-\frac{a}{2}\right)=TVI_j\left(r,\beta_j+\frac{b}{2}\right) \quad (32b)$$

$$qIV_{\theta,i}\left(r,\alpha_i+\frac{c}{2}\right)=qVII_{\theta,i}\left(r,\gamma_i-\frac{d}{2}\right) \quad (33a)$$

$$qIV_{\theta,i}\left(r,\alpha_i-\frac{c}{2}\right)=qVII_{\theta,i}\left(r,\gamma_i+\frac{d}{2}\right) \quad (33b)$$

$$TIV_i\left(r,\alpha_i+\frac{c}{2}\right)=TVII_i\left(r,\gamma_i-\frac{d}{2}\right) \quad (34a)$$

$$TIV_i\left(r,\alpha_i-\frac{c}{2}\right)=TVII_i\left(r,\gamma_i+\frac{d}{2}\right) \quad (34b)$$

When the heat transfer by convection in the air-gap is considered, the ICs **(21)**, **(22)**, **(24)** and **(25)** are modified respectively by

$$qII_{r,j}\left(R_m,\theta\right)=h_e\left(TII_j\left(R_m,\theta\right)-TI\left(R_m,\theta\right)\right) \quad (35)$$

$$qVI_{r,j}\left(R_m,\theta\right)=h_e\left(TVI_j\left(R_m,\theta\right)-TI\left(R_m,\theta\right)\right) \quad (36)$$

$$qIV_{r,i}\left(R_s,\theta\right)=-h_e\left(TIV_i\left(R_s,\theta\right)-TI\left(R_s,\theta\right)\right) \quad (37)$$

$$qVII_{r,i}\left(R_s,\theta\right)=-h_e\left(TVII_i\left(R_s,\theta\right)-TI\left(R_s,\theta\right)\right) \quad (38)$$

where h_e is the coefficient of convection in the air gap (in W/m^2K).

The heat transfer in the *θ*- and *r*-directions by convection between air regions and solid regions of the machine can be introduced in the analytical model in the same way. This situation can be found in the SPM with air space between PMs.

Outside the stator and inside the rotor, the heat transfer by radiation can occur and can be taken into account by modifying **(17)** and **(30)** respectively by

$$qV_r\left(R_i,\theta\right)=-h_r\left(TV\left(R_i,\theta\right)-T_{\text{int}}\right)-\varepsilon\sigma\left(TV^4\left(R_i,\theta\right)-T_{\text{int}}^4\right) \quad (39)$$

$$qIII_r\left(R_{ext},\theta\right)=h_s\left(TIII\left(R_{ext},\theta\right)-T_{ext}\right)+\varepsilon\sigma\left(TIII^4\left(R_{ext},\theta\right)-T_{ext}^4\right) \quad (40)$$

where h_r and h_s are respectively the coefficient of convection inside the rotor and outside the stator, ε the emissivity coefficient, and σ the Boltzmann constant. In this paper, we consider only convection outside the stator and inside the rotor.

All above ICs consider that the contact between regions is perfect. In electrical machines, there are some regions where the interfaces contact is not perfect. This is the case for example of SPM with PMs mounted at the surface of rotor using glue. In this case, IC **(18)** is modified as

$$qV_r\left(R_r,\theta\right)=\frac{1}{R_c}\left(TV\left(R_r,\theta\right)-TII_j\left(R_r,\theta\right)\right) \quad (41)$$

where R_c is the contact resistance between PMs and the rotor yoke due to glue (in m^2K/W).

In the case of Spoke machine where Region V does not exist, the convective BC at the rotor shaft is applied directly to PMs and rotor teeth regions [see **Fig. 1(d)**]. The ICs at $r=R_r$ are

$$qII_{r,j}\left(R_r,\theta\right)=-h_r\left(TII_j\left(R_r,\theta\right)-T_{\text{int}}\right) \quad (42)$$

$$qVI_{r,j}\left(R_r,\theta\right)=-h_r\left(TVI_j\left(R_r,\theta\right)-T_{\text{int}}\right) \quad (43)$$

D. Development of Interface Conditions

The development of ICs permits to obtain a system of equations whose unknowns are the coefficients of Fourier's series solution in each subdomain. The resolution of this system gives the distribution of temperature and heat flux in the entire machine. In this section, we develop only the ICs of the conduction problem [i.e., **(17)** to **(34b)**] with convective heat transfer to ambient air and at the rotor.

The development of ICs for the introduction of convection in the air-gap [i.e., **(35)** to **(38)**], the radiation outside the stator and inside the rotor [i.e., **(39)** and **(40)**], the contact resistance between subdomains for non-perfect contact [i.e., **(41)**], and convective BC in the rotor for Spoke machine [i.e., **(42)** and **(43)**] can be done easily in the same way as in the conduction problem.

In the *θ*-direction, the IC **(17)**, which represents the interface of heat transfer by convection inside the rotor, gives 3 equations

$$\lambda_r\left(-\frac{p_rR_i}{2\lambda_r}+\frac{A9_0}{R_i}\right)=h_r\left(-\frac{p_rR_i^2}{4\lambda_r}+A9_0\ln\left(R_i\right)+A10_0-T_{\text{int}}\right) \quad (44)$$

$$\frac{n\lambda_r}{R_i}\left(A9_n-A10_n\right)=h_r\left(A9_n+A10_n\right) \quad (45)$$

$$\frac{n\lambda_r}{R_i}\left(A11_n - A12_n\right) = h_r\left(A11_n + A12_n\right) \tag{46}$$

From IC **(18)**, which represents the perfect contact between PMs and the rotor yoke, we obtain 2 equations

$$B1_{j,0} + B2_{j,0}\ln\left(R_r\right) - \frac{Pm_j R_r^2}{4\lambda_m} = \frac{1}{a}\int_{g_j-\frac{a}{2}}^{g_j+\frac{a}{2}} TV\left(R_r,\theta\right)d\theta \tag{47}$$

$$B1_{j,m}\left(\frac{R_r}{R_m}\right)^{\frac{m\pi}{a}} + B2_{j,m} = \frac{2}{a}\int_{g_j-\frac{a}{2}}^{g_j+\frac{a}{2}} TV\left(R_r,\theta\right)\cos\left(\frac{m\pi}{a}\left(\theta - g_j + \frac{a}{2}\right)\right)d\theta \tag{48}$$

From IC **(19)**, which represents the perfect contact between rotor yoke and rotor teeth (or air space in the SPM), we obtained 2 equations

$$B6_{j,0} + B5_{j,0}\ln\left(R_r\right) - \frac{Pdr_j R_r^2}{4\lambda_a} = \frac{1}{b}\int_{\beta_j-\frac{b}{2}}^{\beta_j+\frac{b}{2}} TV\left(R_r,\theta\right)d\theta \tag{49}$$

$$B5_{j,m}\left(\frac{R_r}{R_m}\right)^{\frac{m\pi}{b}} + B6_{j,m} = \frac{2}{b}\int_{\beta_j-\frac{b}{2}}^{\beta_j+\frac{b}{2}} TV\left(R_r,\theta\right)\cos\left(\frac{m\pi}{b}\left(\theta - \beta_j + \frac{b}{2}\right)\right)d\theta \tag{50}$$

The heat flux transfer in IC **(20)** between Regions V, IIj and VIj permit to obtain 3 equations as

$$-\lambda_r\left(-\frac{p_r R_r}{2\lambda_r} + \frac{A9_0}{R_r}\right) = \frac{1}{2\pi}\sum_{j=1}^{2p}\int_{g_j-\frac{a}{2}}^{g_j+\frac{a}{2}} qII_{r,j}\left(R_r,\theta\right)d\theta \cdots + \frac{1}{2\pi}\sum_{j=1}^{2p}\int_{\beta_j-\frac{b}{2}}^{\beta_j+\frac{b}{2}} qVI_{r,j}\left(R_r,\theta\right)d\theta \tag{51}$$

where p is the number of poles pairs.

$$-\frac{\lambda_r n}{R_r}\left(A9_n\left(\frac{R_r}{R_i}\right)^n \cdots - A10_n\left(\frac{R_r}{R_i}\right)^{-n}\right) = \frac{1}{\pi}\sum_{j=1}^{2p}\int_{g_j-\frac{a}{2}}^{g_j+\frac{a}{2}} qII_{r,j}\left(R_r,\theta\right)\cos\left(n\theta\right)d\theta \cdots + \frac{1}{\pi}\sum_{j=1}^{2p}\int_{\beta_j-\frac{b}{2}}^{\beta_j+\frac{b}{2}} qVI_{r,j}\left(R_r,\theta\right)\cos\left(n\theta\right)d\theta \tag{52}$$

$$-\frac{\lambda_r n}{R_r}\left(A11_n\left(\frac{R_r}{R_i}\right)^n \cdots - A12_n\left(\frac{R_r}{R_i}\right)^{-n}\right) = \frac{1}{\pi}\sum_{j=1}^{2p}\int_{g_j-\frac{a}{2}}^{g_j+\frac{a}{2}} qII_{r,j}\left(R_r,\theta\right)\sin\left(n\theta\right)d\theta \cdots + \frac{1}{\pi}\sum_{j=1}^{2p}\int_{\beta_j-\frac{b}{2}}^{\beta_j+\frac{b}{2}} qVI_{r,j}\left(R_r,\theta\right)\sin\left(n\theta\right)d\theta \tag{53}$$

The IC **(21)** between temperatures of the air-gap and PMs, we have

$$B1_{j,0} + B2_{j,0}\ln\left(R_m\right) - \frac{Pm_j R_m^2}{4\lambda_m} = \frac{1}{a}\int_{g_j-\frac{a}{2}}^{g_j+\frac{a}{2}} TI\left(R_m,\theta\right)d\theta \tag{54}$$

$$B1_{j,m} + B2_{j,m}\left(\frac{R_m}{R_r}\right)^{-\frac{m\pi}{a}} = \frac{2}{a}\int_{g_j-\frac{a}{2}}^{g_j+\frac{a}{2}} TI\left(R_m,\theta\right)\cos\left(\frac{m\pi}{a}\left(\theta - g_j + \frac{a}{2}\right)\right)d\theta \tag{55}$$

The IC **(22)**, which represents the perfect contact between air-gap and rotor teeth (or air space between PMs in the SPM), we have

$$B6_{j,0} + B5_{j,0}\ln\left(R_m\right) - \frac{Pdr_j R_m^2}{4\lambda_a} = \frac{1}{b}\int_{\beta_j-\frac{b}{2}}^{\beta_j+\frac{b}{2}} TI\left(R_m,\theta\right)d\theta \tag{56}$$

$$B6_{j,m}\left(\frac{R_m}{R_r}\right)^{-\frac{m\pi}{b}} + B5_{j,m} = \frac{2}{b}\int_{\beta_j-\frac{b}{2}}^{\beta_j+\frac{b}{2}} TI\left(R_m,\theta\right)\cos\left(\frac{m\pi}{b}\left(\theta - \beta_j + \frac{b}{2}\right)\right)d\theta \tag{57}$$

The heat flux continuity in IC **(23)** permits to get 3 equations

$$-\frac{\lambda_e A2_0}{R_m} = \frac{1}{2\pi}\sum_{j=1}^{2p}\int_{g_j-\frac{a}{2}}^{g_j+\frac{a}{2}} qII_{r,j}\left(R_m,\theta\right)d\theta \cdots + \frac{1}{2\pi}\sum_{j=1}^{2p}\int_{\beta_j-\frac{b}{2}}^{\beta_j+\frac{b}{2}} qVI_{r,j}\left(R_m,\theta\right)d\theta \tag{58}$$

$$-\frac{\lambda_e n}{R_m}\left(A3_n\left(\frac{R_m}{R_s}\right)^n \cdots - A4_n\right) = \frac{1}{\pi}\sum_{j=1}^{2p}\int_{g_j-\frac{a}{2}}^{g_j+\frac{a}{2}} qII_{r,j}\left(R_m,\theta\right)\cos\left(n\theta\right)d\theta \cdots + \frac{1}{\pi}\sum_{j=1}^{2p}\int_{\beta_j-\frac{b}{2}}^{\beta_j+\frac{b}{2}} qVI_{r,j}\left(R_m,\theta\right)\cos\left(n\theta\right)d\theta \tag{59}$$

$$-\frac{\lambda_e n}{R_m}\left(A1_n\left(\frac{R_m}{R_s}\right)^n \cdots - A2_n\right) = \frac{1}{\pi}\sum_{j=1}^{2p}\int_{g_j-\frac{a}{2}}^{g_j+\frac{a}{2}} qII_{r,j}\left(R_m,\theta\right)\sin\left(n\theta\right)d\theta \cdots + \frac{1}{\pi}\sum_{j=1}^{2p}\int_{\beta_j-\frac{b}{2}}^{\beta_j+\frac{b}{2}} qVI_{r,j}\left(R_m,\theta\right)\sin\left(n\theta\right)d\theta \tag{60}$$

The IC **(24)** between air-gap and stator slots gives

$$C1_{i,0} + C2_{i,0}\ln\left(R_s\right) - \frac{Psl_i R_s^2}{4\lambda_{sl}} = \frac{1}{c}\int_{\alpha_i-\frac{c}{2}}^{\alpha_i+\frac{c}{2}} TI\left(R_s,\theta\right)d\theta \tag{61}$$

$$C1_{i,m1}\left(\frac{R_s}{r_4}\right)^{\frac{m1\pi}{c}} + C2_{i,m1} = \frac{2}{c}\int_{\alpha_i-\frac{c}{2}}^{\alpha_i+\frac{c}{2}} TI\left(R_s,\theta\right)\cos\left(\frac{m1\pi}{c}\left(\theta - \alpha_i + \frac{c}{2}\right)\right)d\theta \tag{62}$$

The IC **(25)** between air gap and stator teeth gives

$$C5_{i,0} + C6_{i,0}\ln\left(R_s\right) - \frac{Pd_i R_s^2}{4\lambda_d} = \frac{1}{d}\int_{\gamma_i-\frac{d}{2}}^{\gamma_i+\frac{d}{2}} TI\left(R_s,\theta\right)d\theta \tag{63}$$

$$C5_{i,m1}\left(\frac{R_s}{r_4}\right)^{\frac{m1\pi}{d}} + C6_{i,m1} = \frac{2}{d}\int_{\gamma_i-\frac{d}{2}}^{\gamma_i+\frac{d}{2}} TI\left(R_s,\theta\right)\cos\left(\frac{m1\pi}{d}\left(\theta - \gamma_i + \frac{d}{2}\right)\right)d\theta \tag{64}$$

The heat flux continuity in IC **(26)** permits to get 3 equations

$$-\frac{\lambda_e A2_0}{R_s} = \frac{1}{2\pi}\sum_{i=1}^{Q_s}\left(\int_{\alpha_i-\frac{c}{2}}^{\alpha_i+\frac{c}{2}} qIV_{r,i}\left(R_s,\theta\right)d\theta + \int_{\gamma_i-\frac{d}{2}}^{\gamma_i+\frac{d}{2}} qVII_{r,i}\left(R_s,\theta\right)d\theta\right) \quad (65)$$

$$-\frac{\lambda_e n}{R_s}\left(A3_n \cdots - A4_n\left(\frac{R_s}{R_m}\right)^{-n}\right) = \frac{1}{\pi}\sum_{i=1}^{Q_s}\int_{\alpha_i-\frac{c}{2}}^{\alpha_i+\frac{c}{2}} qIV_{r,i}\left(R_s,\theta\right)\cos\left(n\theta\right)d\theta \cdots + \frac{1}{\pi}\sum_{i=1}^{Q_s}\int_{\gamma_i-\frac{d}{2}}^{\gamma_i+\frac{d}{2}} qVII_{r,i}\left(R_s,\theta\right)\cos\left(n\theta\right)d\theta \quad (66)$$

$$-\frac{\lambda_e n}{R_s}\left(A1_n \cdots - A2_n\left(\frac{R_s}{R_m}\right)^{-n}\right) = \frac{1}{\pi}\sum_{i=1}^{Q_s}\int_{\alpha_i-\frac{c}{2}}^{\alpha_i+\frac{c}{2}} qIV_{r,i}\left(R_s,\theta\right)\sin\left(n\theta\right)d\theta \cdots + \frac{1}{\pi}\sum_{i=1}^{Q_s}\int_{\gamma_i-\frac{d}{2}}^{\gamma_i+\frac{d}{2}} qVII_{r,i}\left(R_s,\theta\right)\sin\left(n\theta\right)d\theta \quad (67)$$

The IC **(27)** between temperatures of stator yoke and stator slots gives

$$C1_{i,0} + C2_{i,0}\ln\left(r_4\right) - \frac{Psl_i r_4^2}{4\lambda_{sl}} = \frac{1}{c}\int_{\alpha_i-\frac{c}{2}}^{\alpha_i+\frac{c}{2}} TIII\left(r_4,\theta\right)d\theta \quad (68)$$

$$C2_{i,m1}\left(\frac{r_4}{R_s}\right)^{-\frac{m1\pi}{c}} + C1_{i,m1} = \frac{2}{c}\int_{\alpha_i-\frac{c}{2}}^{\alpha_i+\frac{c}{2}} TIII\left(r_4,\theta\right)\cos\left(\frac{m1\pi}{c}\left(\theta-\alpha_i+\frac{c}{2}\right)\right)d\theta \quad (69)$$

The IC **(28)** between temperatures of stator yoke and stator teeth gives

$$C5_{i,0} + C6_{i,0}\ln\left(r_4\right) - \frac{Pd_i r_4^2}{4\lambda_d} = \frac{1}{d}\int_{\gamma_i-\frac{d}{2}}^{\gamma_i+\frac{d}{2}} TIII\left(r_4,\theta\right)d\theta \quad (70)$$

$$C6_{i,m1}\left(\frac{r_4}{R_s}\right)^{-\frac{m1\pi}{d}} + C5_{i,m1} = \frac{2}{d}\int_{\gamma_i-\frac{d}{2}}^{\gamma_i+\frac{d}{2}} TIII\left(r_4,\theta\right)\cos\left(\frac{m1\pi}{d}\left(\theta-\gamma_i+\frac{d}{2}\right)\right)d\theta \quad (71)$$

In conduction problems, the heat flux continuity between stator yoke, stator slots and stator teeth is represented by IC **(29)** giving

$$-\lambda_s\left(-\frac{p_s r_4}{2\lambda_s} \cdots + \frac{A5_0}{r_4}\right) = \frac{1}{2\pi}\sum_{i=1}^{Q_s}\left(\int_{\alpha_i-\frac{c}{2}}^{\alpha_i+\frac{c}{2}} qIV_{r,i}\left(r_4,\theta\right)d\theta + \int_{\gamma_i-\frac{d}{2}}^{\gamma_i+\frac{d}{2}} qVII_{r,i}\left(r_4,\theta\right)d\theta\right) \quad (72)$$

$$-\frac{\lambda_s n}{r_4}\left(A5_n\left(\frac{r_4}{R_{ext}}\right)^{n} \cdots - A6_n\left(\frac{r_4}{R_{ext}}\right)^{-n}\right) = \frac{1}{\pi}\sum_{i=1}^{Q_s}\int_{\alpha_i-\frac{c}{2}}^{\alpha_i+\frac{c}{2}} qIV_{r,i}\left(r_4,\theta\right)\cos\left(n\theta\right)d\theta \cdots + \frac{1}{\pi}\sum_{i=1}^{Q_s}\int_{\gamma_i-\frac{d}{2}}^{\gamma_i+\frac{d}{2}} qVII_{r,i}\left(r_4,\theta\right)\cos\left(n\theta\right)d\theta \quad (73)$$

$$-\frac{\lambda_s n}{r_4}\left(A7_n\left(\frac{r_4}{R_{ext}}\right)^{n} \cdots - A8_n\left(\frac{r_4}{R_{ext}}\right)^{-n}\right) = \frac{1}{\pi}\sum_{i=1}^{Q_s}\int_{\alpha_i-\frac{c}{2}}^{\alpha_i+\frac{c}{2}} qIV_{r,i}\left(r_4,\theta\right)\sin\left(n\theta\right)d\theta \cdots + \frac{1}{\pi}\sum_{i=1}^{Q_s}\int_{\gamma_i-\frac{d}{2}}^{\gamma_i+\frac{d}{2}} qVII_{r,i}\left(r_4,\theta\right)\sin\left(n\theta\right)d\theta \quad (74)$$

The heat transfer by convection between stator and air ambient outside the stator, which is represented by IC **(30)**, gives 3 equations

$$-\lambda_s\left(-\frac{p_s R_{ext}}{2\lambda_s} + \frac{A5_0}{R_{ext}}\right) = h_s\left(-\frac{p_s R_{ext}^2}{4\lambda_s} + A5_0\ln\left(R_{ext}\right) + A6_0 - T_{ext}\right) \quad (75)$$

$$-\frac{n\lambda_s}{R_{ext}}\left(A5_n - A6_n\right) = h_s\left(A5_n + A6_n\right) \quad (76)$$

$$-\frac{n\lambda_s}{R_{ext}}\left(A7_n - A8_n\right) = h_s\left(A7_n + A8_n\right) \quad (77)$$

In the *r*-direction, the heat flux continuity represented by IC **(31a)** permits to get

$$\frac{k\pi\lambda_m}{gg\cdot sh\left(\frac{k\pi a}{gg}\right)}\left(B3_{j,k}\,ch\left(\frac{k\pi a}{gg}\right) \cdots + B4_{j,k}\right) = \frac{k\pi\lambda_a}{gg\cdot sh\left(\frac{k\pi b}{gg}\right)}\left(B8_{j,k}\,ch\left(\frac{k\pi b}{gg}\right) \cdots + B7_{j,k}\right) \quad (78)$$

The IC **(31b)** permits to get $2p$ equations. For the first PM (or rotor cage bar), we have

$$\frac{k\pi\lambda_m}{gg\cdot sh\left(\frac{k\pi a}{gg}\right)}\left(B4_{1,k}\,ch\left(\frac{k\pi a}{gg}\right) \cdots + B3_{1,k}\right) = \frac{k\pi\lambda_a}{gg\cdot sh\left(\frac{k\pi b}{gg}\right)}\left(B7_{2p,k}\,ch\left(\frac{k\pi b}{gg}\right) \cdots + B8_{2p,k}\right) \quad (79)$$

For the other $2p-1$ PM (with *j* vary from 2 to $2p$), we obtain

$$\frac{k\pi\lambda_m}{gg\cdot sh\left(\frac{k\pi a}{gg}\right)}\left(B4_{j,k}\,ch\left(\frac{k\pi a}{gg}\right) \cdots + B3_{j,k}\right) = \frac{k\pi\lambda_a}{gg\cdot sh\left(\frac{k\pi b}{gg}\right)}\left(B7_{j-1,k}\,ch\left(\frac{k\pi b}{gg}\right) \cdots + B8_{j-1,k}\right) \quad (80)$$

The IC **(32a)** between temperatures of PM (or cage bar in the IM) and rotor teeth (or air between PMs in the SPM) gives

$$-\left(B8_{j,k} + B3_{j,k}\right) = \frac{2}{gg}\left(\left(-B5_{j,0} + B2_{j,0}\right)\mathrm{int}\,2 + \left(B1_{j,0} - B6_{j,0}\right)\mathrm{int}\,1 + \left(-\frac{Pm_j}{4\lambda_m} + \frac{Pdr_j}{4\lambda_a}\right)\mathrm{int}\,7\right) \cdots + \frac{2}{gg}\sum_{m=1}^{mm}\left(-B5_{j,m}\,\mathrm{int}\,3 - B6_{j,m}\,\mathrm{int}\,4 + \cos\left(m\pi\right)\left(B1_{j,m}\,\mathrm{int}\,5 + B2_{j,m}\,\mathrm{int}\,6\right)\right) \quad (81)$$

Development of IC **(32b)** for the first PM (or cage rotor bar) and rotor teeth (or air between PMs in the SPM) gives

$$\begin{aligned} B7_{2p,k}+B4_{1,k} &= \frac{2}{gg}\left(\left(-B5_{2p,0}+B2_{1,0}\right)\text{int}\,2+\left(B1_{1,0}-B6_{2p,0}\right)\text{int}\,1+\left(-\frac{Pm_1}{4\lambda_m}+\frac{Pdr_{2p}}{4\lambda_a}\right)\text{int}\,7\right. \\ &\cdots+\frac{2}{gg}\sum_{m=1}^{mm}\left.\left(-\left(B5_{2p,m}\,\text{int}\,3+B6_{2p,m}\,\text{int}\,4\right)\cos\left(m\pi\right)+B1_{1,m}\,\text{int}\,5+B2_{1,m}\,\text{int}\,6\right)\right. \end{aligned} \tag{82}$$

For the other $2p-1$ PM, we obtain

$$\begin{aligned} B7_{j,k}+B4_{j+1,k} &= \frac{2}{gg}\left(\left(-B5_{j,0}+B2_{j+1,0}\right)\text{int}\,2+\left(B1_{j+1,0}-B6_{j,0}\right)\text{int}\,1+\left(-\frac{Pm_{j+1}}{4\lambda_m}+\frac{Pdr_j}{4\lambda_a}\right)\text{int}\,7\right. \\ &\cdots+\frac{2}{gg}\sum_{m=1}^{mm}\left.\left(\left(B5_{j,m}\,\text{int}\,3+B6_{j,m}\,\text{int}\,4\right)\cos\left(m\pi\right)+B1_{j+1,m}\,\text{int}\,5+B2_{j+1,m}\,\text{int}\,6\right)\right. \end{aligned} \tag{83}$$

where $\text{int}\,1=\int_{R_r}^{R_m}\frac{1}{r}\sin\left(\frac{k\pi}{gg}\ln\left(\frac{r}{R_r}\right)\right)dr$, $\text{int}\,2=\int_{R_r}^{R_m}\frac{\ln(r)}{r}\sin\left(\frac{k\pi}{gg}\ln\left(\frac{r}{R_r}\right)\right)dr$, $\text{int}\,3=\int_{R_r}^{R_m}\frac{1}{r}\sin\left(\frac{k\pi}{gg}\ln\left(\frac{r}{R_r}\right)\right)\left(\frac{r}{R_m}\right)^{\frac{m\pi}{b}}dr$, $\text{int}\,4=\int_{R_r}^{R_m}\frac{1}{r}\sin\left(\frac{k\pi}{gg}\ln\left(\frac{r}{R_r}\right)\right)\left(\frac{r}{R_r}\right)^{-\frac{m\pi}{b}}dr$, $\text{int}\,5=\int_{R_r}^{R_m}\frac{1}{r}\sin\left(\frac{k\pi}{gg}\ln\left(\frac{r}{R_r}\right)\right)\left(\frac{r}{R_m}\right)^{\frac{m\pi}{a}}dr$, $\text{int}\,6=\int_{R_r}^{R_m}\frac{1}{r}\sin\left(\frac{k\pi}{gg}\ln\left(\frac{r}{R_r}\right)\right)\left(\frac{r}{R_r}\right)^{-\frac{m\pi}{a}}dr$, and $\text{int}\,7=\int_{R_r}^{R_m}r\sin\left(\frac{k\pi}{gg}\ln\left(\frac{r}{R_r}\right)\right)dr$.

For the stator slots and stator teeth, the development of IC **(34a)** gives

$$\begin{aligned} C3_{i,k1}+C8_{i,k1} &= \frac{2}{ff}\left(\left(-C2_{i,0}+C6_{i,0}\right)\text{int}\,2s+\left(C5_{i,0}-C1_{i,0}\right)\text{int}\,1s+\left(-\frac{Pd_i}{4\lambda_d}+\frac{Psl_i}{4\lambda_{sl}}\right)\text{int}\,7s\right. \\ &\cdots+\frac{2}{ff}\sum_{m1=1}^{mm1}\left.\left(C5_{i,m1}\,\text{int}\,3s+C6_{i,m1}\,\text{int}\,4s-\cos\left(m1\pi\right)\left(C1_{i,m1}\,\text{int}\,5s+C2_{i,m1}\,\text{int}\,6s\right)\right)\right. \end{aligned} \tag{84}$$

Development of IC **(34b)** for the first stator slot and the last stator tooth permits to get

$$\begin{aligned} -C4_{1,k1}-C7_{Q_s,k1} &= \frac{2}{ff}\left(\left(-C2_{1,0}+C6_{Q_s,0}\right)\text{int}\,2s+\left(C5_{Q_s,0}-C1_{1,0}\right)\text{int}\,1s+\left(-\frac{Pd_{Q_s}}{4\lambda_d}+\frac{Psl_1}{4\lambda_{sl}}\right)\text{int}\,7s\right. \\ &\cdots+\frac{2}{ff}\sum_{m1=1}^{mm1}\left.\left(\left(C5_{Q_s,m1}\,\text{int}\,3s+C6_{Q_s,m1}\,\text{int}\,4s\right)\cos\left(m1\pi\right)-C1_{1,m1}\,\text{int}\,5s-C2_{1,m1}\,\text{int}\,6s\right)\right. \end{aligned} \tag{85}$$

For the other stator slots and stator teeth (with *i* vary from 1 to Q_s-1), we have

$$\begin{aligned} -C7_{i,k1}-C4_{i+1,k1} &= \frac{2}{ff}\left(\left(-C2_{i+1,0}+C6_{i,0}\right)\text{int}\,2s+\left(-C1_{i+1,0}+C5_{i,0}\right)\text{int}\,1s+\left(-\frac{Pd_i}{4\lambda_d}+\frac{Psl_{i+1}}{4\lambda_{sl}}\right)\text{int}\,7s\right. \\ &\cdots+\frac{2}{ff}\sum_{m1=1}^{mm1}\left.\left(\left(C5_{i,m1}\,\text{int}\,3s+C6_{i,m1}\,\text{int}\,4s\right)\cos\left(m1\pi\right)-C1_{i+1,m1}\,\text{int}\,5s-C2_{i+1,m1}\,\text{int}\,6s\right)\right. \end{aligned} \tag{86}$$

The integrals in the stator slots and teeth in the *r*-direction $\text{int}\,1s \sim \text{int}\,7s$ between R_s and r_4 are similar to above integrals at the rotor subdomains between R_r and R_m. In the θ-direction, the integrals are simple and easy to calculate.

The heat flux continuity between stator slots and stator teeth is represented by IC **(33a)** giving

$$\frac{k1\pi\lambda_{sl}}{ff.sh\left(\frac{k1\pi c}{ff}\right)}\left(\begin{aligned}&C3_{i,k1}ch\left(\frac{k1\pi c}{ff}\right)\\&\cdots+C4_{i,k1}\end{aligned}\right)=\frac{k1\pi\lambda_d}{ff.sh\left(\frac{k1\pi d}{ff}\right)}\left(\begin{aligned}&C8_{i,k1}ch\left(\frac{k1\pi d}{ff}\right)\\&\cdots+C7_{i,k1}\end{aligned}\right) \tag{87}$$

The IC **(33b)** gives Q_s equations. For the first stator slot, we have

$$\frac{k1\pi\lambda_{sl}}{ff.sh\left(\frac{k1\pi c}{ff}\right)}\left(\begin{aligned}&C4_{1,k1}ch\left(\frac{k1\pi c}{ff}\right)\\&\cdots+C3_{1,k1}\end{aligned}\right)=\frac{k1\pi\lambda_d}{ff.sh\left(\frac{k1\pi d}{ff}\right)}\left(\begin{aligned}&C7_{Q_s,k1}ch\left(\frac{k1\pi d}{ff}\right)\\&\cdots+C8_{Q_s,k1}\end{aligned}\right) \tag{88}$$

For the other Q_s-1 slots (with *i* vary from 2 to Q_s), we obtain

$$\frac{k1\pi\lambda_{sl}}{ff.sh\left(\frac{k1\pi c}{ff}\right)}\left(\begin{aligned}&C4_{i,k1}ch\left(\frac{k1\pi c}{ff}\right)\\&\cdots+C3_{i,k1}\end{aligned}\right)=\frac{k1\pi\lambda_d}{ff.sh\left(\frac{k1\pi d}{ff}\right)}\left(\begin{aligned}&C7_{i-1,k1}ch\left(\frac{k1\pi d}{ff}\right)\\&\cdots+C8_{i-1,k1}\end{aligned}\right) \tag{89}$$

III. Temperature and Heat Flux Results

The parameters and dimensions of the studied electrical machines are given in **Table I**. The machines have a simple distributed 4 poles winding. The power losses of SPM and IPM at 500 *rpm* used as sources for the thermal model are calculated using simple formulas presented in **[27]**. The *B(H)* curve of stator and rotor iron for the electromagnetic power losses determination by Fem is given in **Fig. 3**. The hysteresis and eddy current coefficients and lamination factor used in losses calculation are also given in **Table I**. For the IM with cage rotor, 6 stator slots and 4 rotor bars are considered to show the validity of the analytical model to predict temperature and heat flux in this type of machines. The heat sources for the IM and Spoke machine are considered the same as in the IPM. The PM losses is considered equal to loss in cage rotor bar. The thermal conductivities, convection coefficients, ambient temperatures and power losses at 500 rpm used in the thermal model are listed in **Table II**. The variation of power losses in the SPM and IPM with speed are shown in **Figs. 4 ~ 5**. The harmonics number of analytical model is nn, mm, kk, $mm1$ and $kk1$ are 200, 50, 50, 40, and 40 respectively. This harmonics number permits to obtain a very good accuracy in comparison with Fem and a reasonable computing time. However, the analytical program is not optimized to compare computational time with Fem. The average number of elements and nodes of the Fem calculation **[22]** are respectively 109,168 and 55,484.

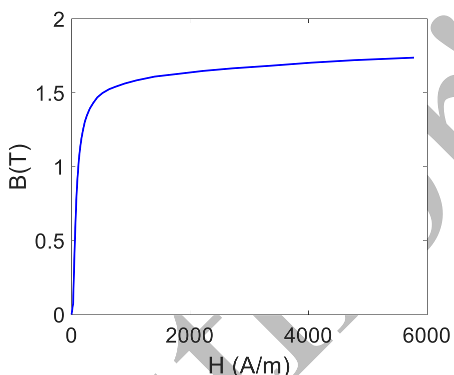

Fig. 3: *B(H)* curve of stator and rotor iron.

TABLE I
Parameters of Studied Machines.

Symbol	Parameters	Value
B_{rm}	Remanence flux density of PMs	1.3 *T*
μ_{rm}	Relative permeability of PMs	1.0277
N_c	Number of conductors per stator slot	23
I_m	Peak phase current	7 *A*
Q_s	Number of stator slots	6
c	Stator slot-opening	30 *deg.*
a	PM-opening	40 *deg.*
p	Number of pole pairs	2
R_{ext}	Radius of the external stator surface	110 *mm*
r_4	Outer radius of stator slot	97 *mm*
R_s	Radius of the stator inner surface	80.5 *mm*
R_m	Radius of the rotor outer surface at the PM	79.7 *mm*
R_r	Radius of the rotor inner surface at the PM	73 *mm*
R_i	Radius of the rotor shaft	40 mm
σ_m	Electrical conductivity of PMs	0.556E6 *S/m*
σ_w	Electrical conductivity of stator coil wires	58E6*S/m*
σ_s	Electrical conductivity of M-19 Steel	1.9E6 *S/m*
c_s	Lamination stacking factor	0.95
c_h	Hysteresis coefficient	143
c_e	Eddy-current coefficient	0.530
g	Air-gap length	0.8 *mm*
L_u	Axial length	40 *mm*
Ω	Mechanical speed	500 *rpm*

TABLE II
Parameters of the Thermal Model.

Symbol	Parameters	Value
λ_e	Thermal conductivity of air-gap	0.03 W/(m ˚K)
λ_a	Thermal conductivity of air	0.03 W/(m ˚K)
λ_m	Thermal conductivity of PMs	9 W/(m ˚K)
λ_s	Thermal conductivity of stator iron	55 W/(m ˚K)
λ_r	Thermal conductivity of rotor iron	55 W/(m ˚K)
λ_b	Thermal conductivity of cage rotor bars	394 W/(m ˚K)
λ_{sl}	Thermal conductivity of stator slot coil	1.73 W/(m ˚K)
p_s	Stator losses in the SPM	4.2 W
p_r	Rotor losses in the SPM	0.17 W
p_m	PM loss in the SPM	6.5 W
p_{sl}	Stator slot losses in the SPM	18.13 *W*
p_s	Stator losses in the IPM	4.07 W
p_r	Rotor losses in the IPM	0.31 W
p_m	PM losses in the IPM	7.94 W
p_{sl}	Stator slot losses in the IPM	18.12 *W*
h_r	Convection coefficient inside the rotor	100 W/(m^2 ˚K)
T_{int}	Temperature inside the rotor	70 ˚C
h_s	Convection coefficient outside the stator	100 W/(m^2 ˚K)
T_{ext}	Temperature outside the stator	70 ˚C

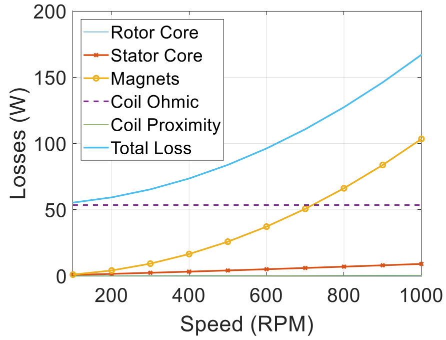

(a)

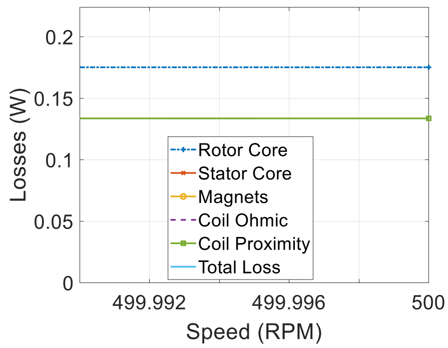

(b)

Fig. 4: Power loss variation with speed in the SPM.

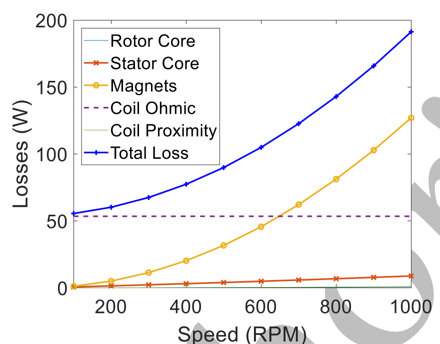

(a)

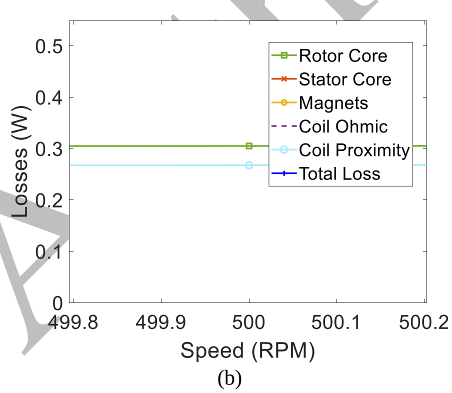

(b)

Fig. 5: Power loss variation with speed in the IPM.

A. *Thermal Results of the SPM and Validation*

For the 6-slots/4-poles SPM, the temperature distribution at speed of 500 *rpm* in the whole machine is shown in **Fig. 6**. We can observe that the temperature is higher inside the stator slots where power loss is higher [see **Table II**]. In the middle of air-gap, the temperature and heat flux components distribution calculated by the developed analytical method and Fem using the parameters and power losses of **Table II** are given in **Fig. 7**.

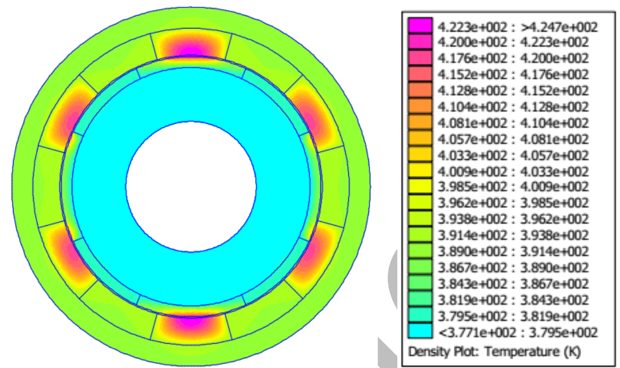

Fig. 6: Temperature distribution in the SPM.

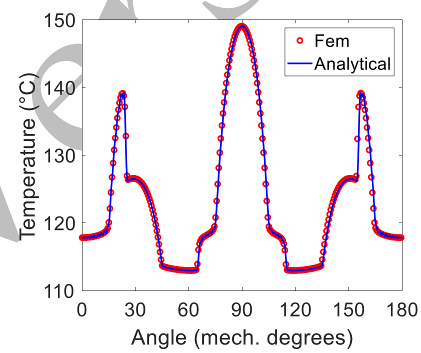

(a)

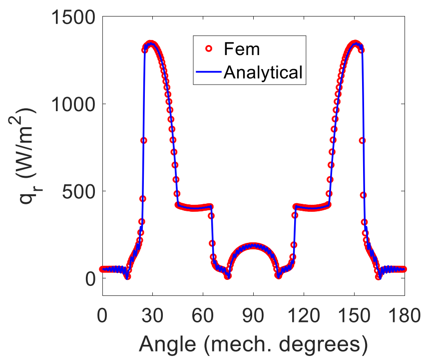

(b)

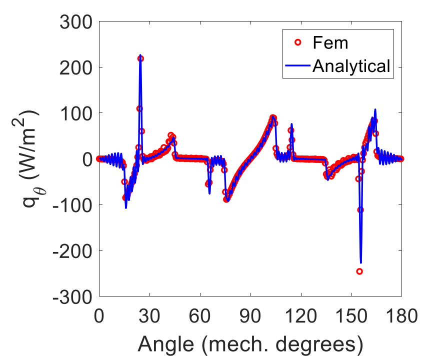

(c)

Fig. 7: Temperature and heat flux components distribution in the middle of air-gap.

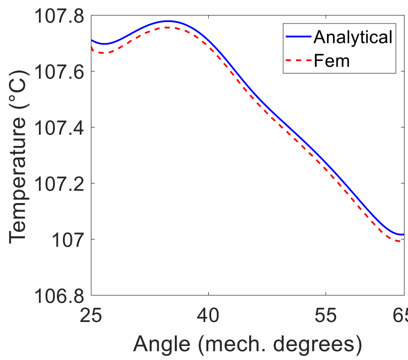

(a) In the θ-direction.

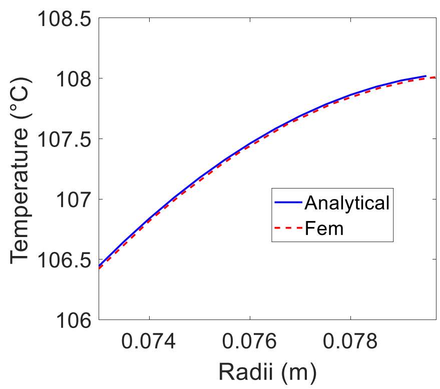

(b) In the r-direction.

Fig. 8: Temperature in the middle of the first PM.

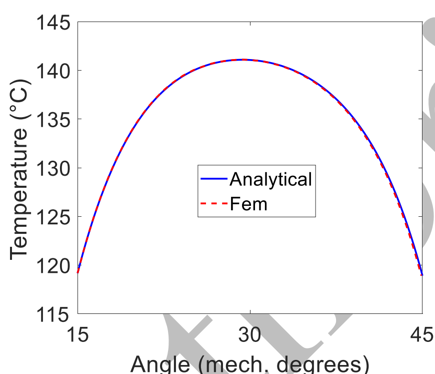

(a) In the θ-direction.

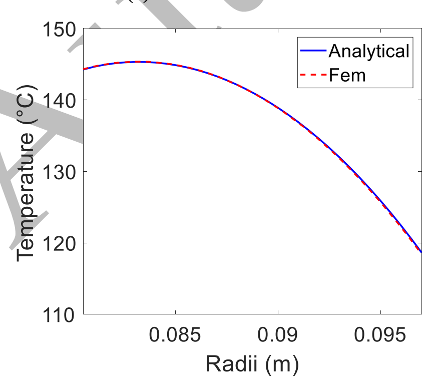

(b) In the r-direction.

Fig. 9: Temperature in the middle of the first stator slot.

To show the ability of the analytical method to predict the temperature distribution in the PMs and the stator slots, the temperature curves in the θ- and r-direction obtained analytically are represented in **Figs. 8 ~ 9** and compared with Fem. The analytical results are in very good agreement with the Fem results. A parametric analysis with varying the convective coefficients h_s and h_r is also done. In **Fig. 10**, the temperature distribution in the machine when the convective coefficients h_s=20 W/(m^2 °K) and h_r=100 W/(m^2 °K) is shown. The corresponding air-gap temperature distribtion is represented in **Fig. 11**. It can be observed that the temperature is higher than the case with h_s=100 W/(m^2 °K). For the case with h_r=20 W/(m^2 °K) and h_s=100 W/(m^2 °K), in **Figs. 12 ~ 13**, we show the temperature distribution in the machine obtained by using Fem and temperature distribution in the middle of air-gap obtained by using the developed analytical method and Fem. In this case also, the analytical results are very close to those of Fem. The variation of temperature in the center of PM and stator slot when the convective coefficients h_s and h_r varies is presented in **Figs. 14 ~ 15**. The comparison of the analytical method results with those obtained by Fem confirms the validity of the proposed analytical method to predict the temperature distribution in the SPM with a very good accuracy.

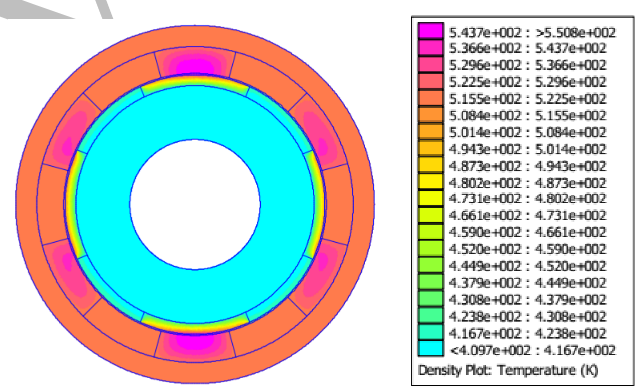

Fig. 10: Temperature distribution in the SPM for h_s=20 W/(m^2 °K) and h_r=100 W/(m^2 °K).

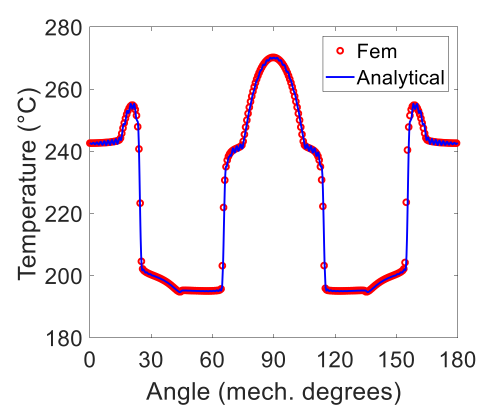

Fig. 11: Temperature distribution in the middle of air-gap for h_s=20 W/(m^2 °K) and h_r=100 W/(m^2 °K).

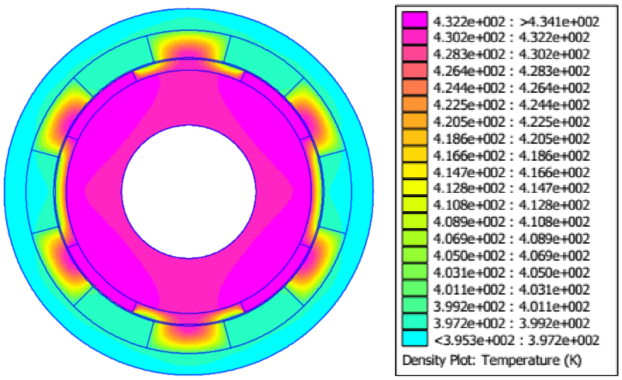

Fig. 12: Temperature distribution in the SPM for h_r=20 W/(m^2 °K) and h_s=100 W/(m^2 °K).

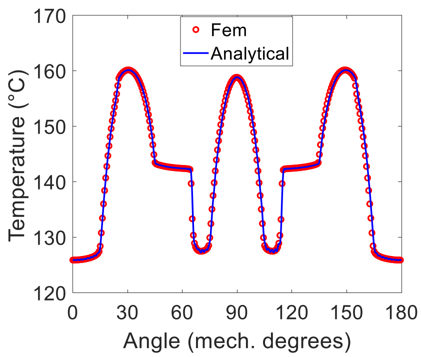

Fig. 13: Temperature distribution in the middle of air-gap for h_r=20 W/(m^2 °K) and h_s=100 W/(m^2 °K).

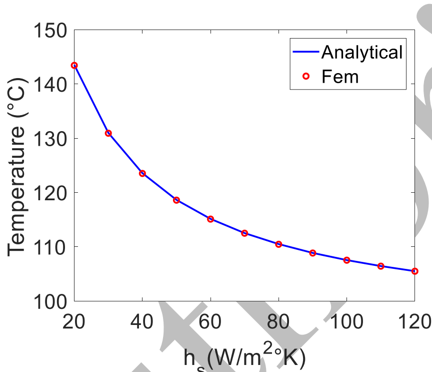

(a) Temperature at the center of the first PM.

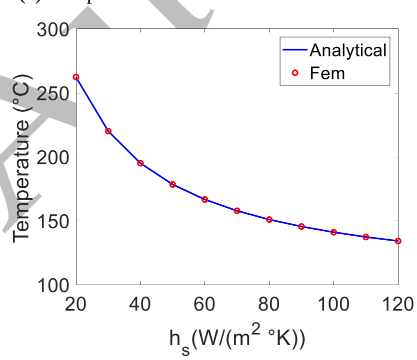

(b) Temperature at the center of the first stator slot.

Fig. 14: Temperature variation with varying h_s and h_r=100 W/(m^2 °K) in a point at the center of PM and stator slot.

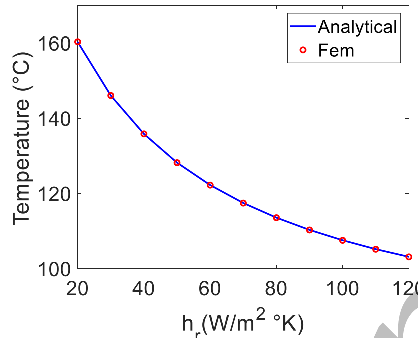

(a) Temperature at the center of the first PM.

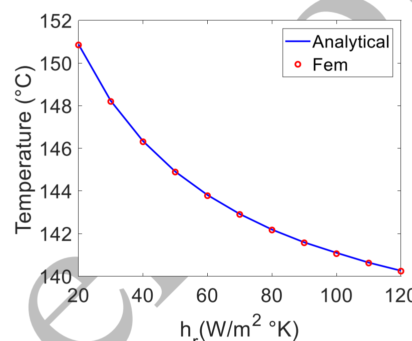

(b) Temperature at the center of the first stator slot.

Fig. 15: Temperature variation with varying h_r and h_s=100 W/(m^2 °K) in a point at the center of PM and stator slot.

B. Thermal Results of the IPM and Validation

Studied IPM machine has the same dimensions and parameters than SPM machine with small difference in power losses [see **Tables I** ~ **II**]. The temperature distribution in the entire machine predicted using Fem is given in **Fig. 16**. The temperature and heat flux components distribution in the middle of air-gap obtained with the analytical method is shown in **Fig. 17**. We can observe a very good agreement between analytical and Fem results. The temperature distribution in the middle of first PM and stator slot in the θ- and r-direction [see **Figs. 18** ~ **19**] obtained analytically and with Fem confirm the accuracy of the proposed analytical method to predict heat transfer in those regions where the effect of temperature is very important.

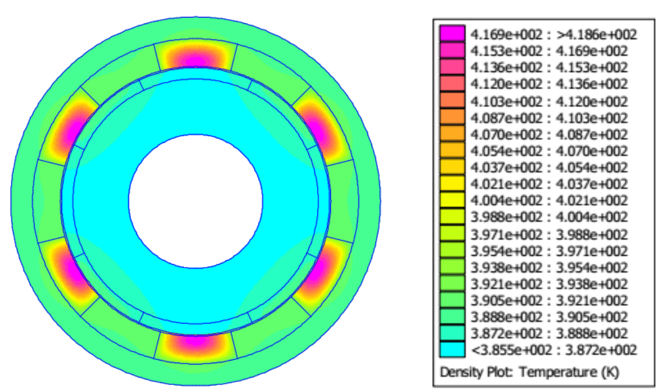

Fig. 16: Temperature distribution in the IPM.

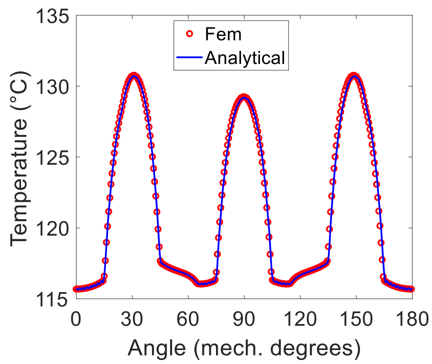

(a)

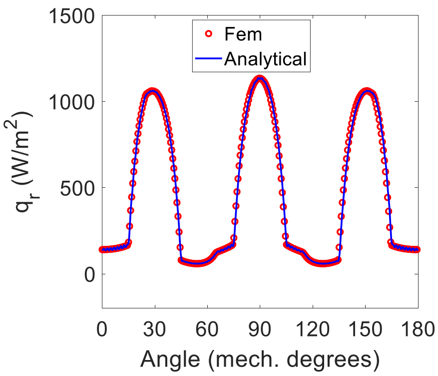

(b)

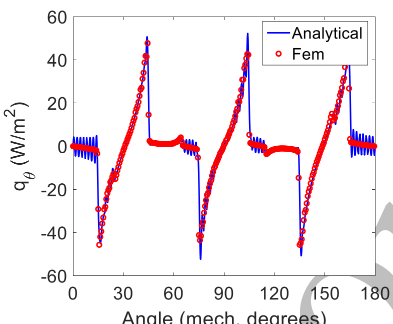

(c)

Fig. 17: Temperature and heat flux components distribution in the middle of air-gap.

When the cooling outside the IPM is not sufficient (h_s=20 W/(m^2 °K)), the heat is not evacuated and the temperature is very high in the stator and air-gap [see **Figs. 20** ~ **21**]. The same observation can be done in the case of not sufficient cooling in the rotor shaft with h_r=20 W/(m^2°K). In this case, the rotor temperature is high but lower than the case of low value of h_s [see **Figs. 22** ~ **23**]. The variation of temperature in the center of first PM and stator slot with the convection coefficient h_s and h_r is represented in **Figs. 45** ~ **25**. Those curves are very important for the design of insulation of stator winding and PM where the characteristics depend on temperature. The effect of convection coefficient of air-gap (i.e., h_e) on the PM and the stator slot is shown in **Figs. 26** ~ **27**. It can be observed that the temperature in the middle of PM decrease with small values of h_e and the temperature in the middle of the stator slot increase for small values of h_e. With low values of convective coefficient in the air-gap, the air-gap is considered as a barrier to heat transfer between stator slot (where the heat source is higher) and PM.

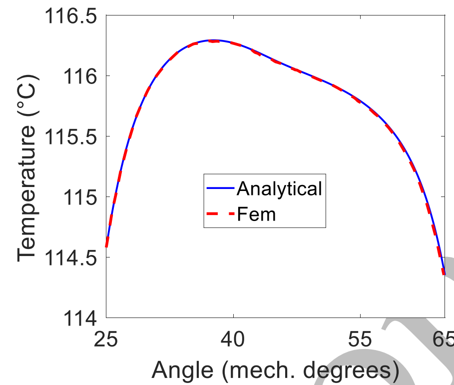

(a) In the θ-direction.

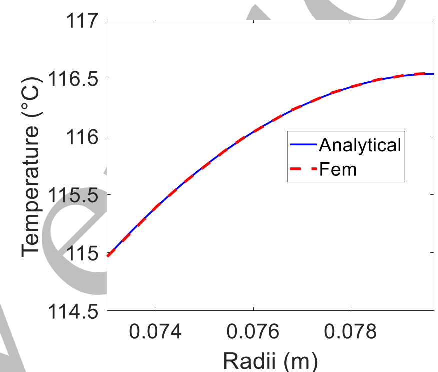

(b) In the r-direction.

Fig. 18: Temperature distribution in the middle of the first PM.

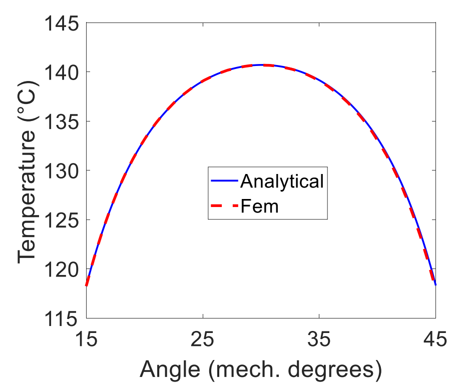

(a) In the θ-direction.

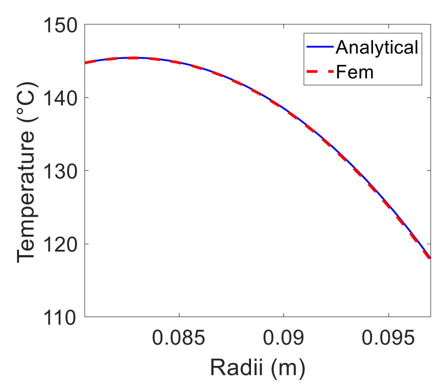

(b) In the r-direction.

Fig. 19: Temperature in the middle of the first stator slot.

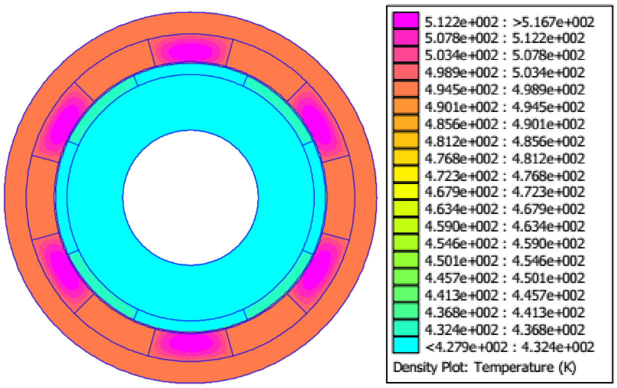

Fig. 20: Temperature distribution in the IPM for h_s=20 W/(m^2 °K) and h_r=100 W/(m^2 °K).

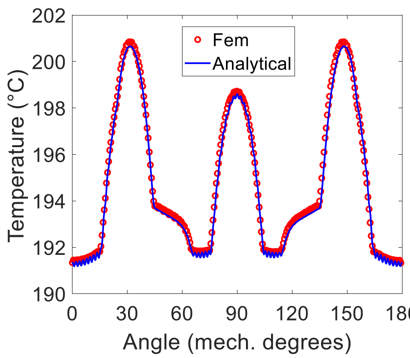

Fig. 21: Temperature distribution in the middle of air-gap for h_s=20 W/(m^2 °K) and h_r=100 W/(m^2 °K).

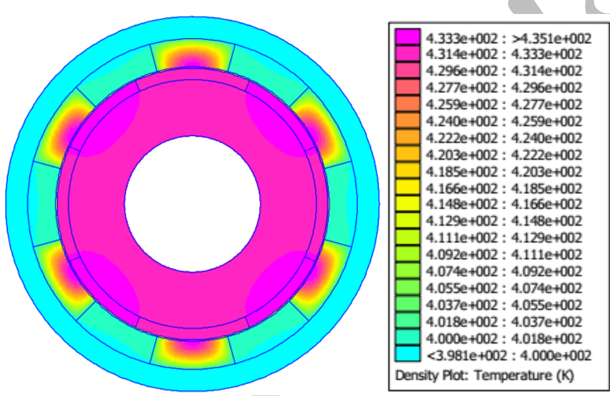

Fig. 22: Temperature distribution in the IPM for h_r=20 W/(m^2 °K) and h_s=100 W/(m^2 °K).

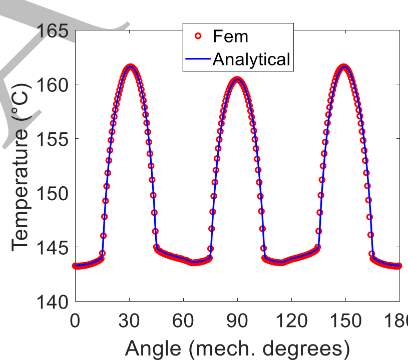

Fig. 23: Temperature distribution in the middle of air-gap for h_r=20 W/(m^2 °K) and h_s=100 W/(m^2 °K).

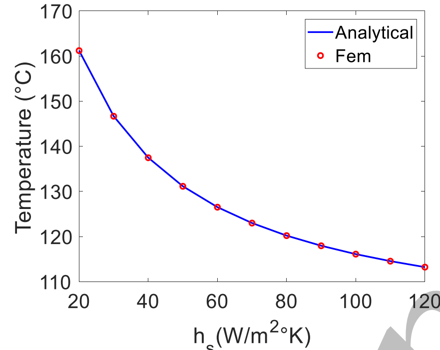

(a) Temperature at the center of the first PM.

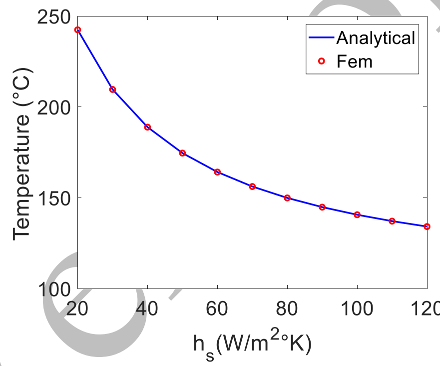

(b) Temperature at the center of the first stator slot.

Fig. 24: Temperature variation with varying h_s and h_r=100 W/(m^2 °K) in a point at the center of PM and stator slot.

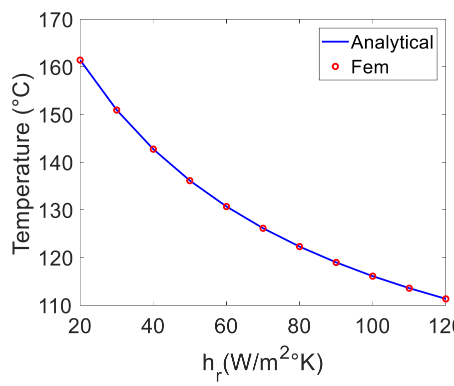

(a) Temperature at the center of the first PM.

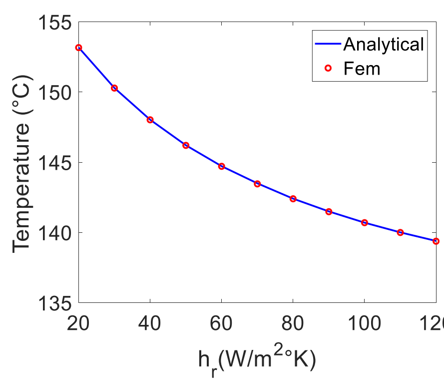

(b) Temperature at the center of the first stator slot.

Fig. 25: Temperature variation with varying h_r and h_s=100 W/(m^2 °K) in a point at the center of PM and stator slot.

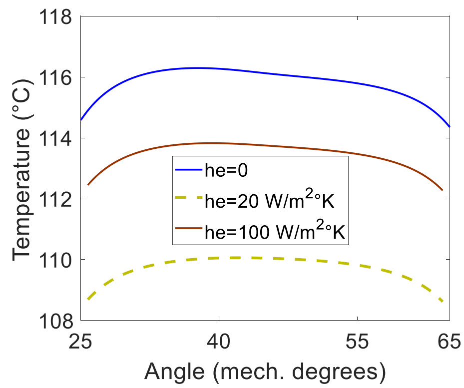

Fig. 26: Analytical temperature distribution in the middle of the first PM with different convective coefficients in the air-gap (with h_s=100 W/(m^2 ˚K) and h_r=100 W/(m^2 ˚K)).

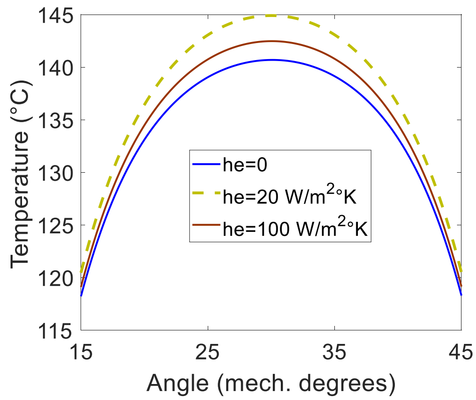

Fig. 27: Analytical temperature distribution in the middle of the first stator slot with different convective coefficients in the air-gap (with h_s=100 W/(m^2°K) and h_r=100 W/(m^2 ˚K)).

C. Thermal Results of the IM and Validation

As explained above, the IM configuration with 6 stator slots and 4 rotor bars studied in this paper does not existe and used only for showing the validity of the proposed analytical model for thermal modeling. The difference between the analyzed IM and IPM in term of thermal modeling is the conductivity of PM and cage rotor bars. This later which is equal to 394 W/(m ˚K) is very high than the conductivity of PM equal to 9 W/(m ˚K). The heat sources in the PMs of the IPM are replaced with the heat sources of cage rotor bar in the IM. The dimensions of cage rotor bars are higher than the dimensions of PMs in this example. The temperature distribution in the machine obtained by using Fem is represented in **Fig. 28**. It can be observed that the essential of heat is located in the stator slots. The temperature and heat flux components distribution in the middle of air-gap is shown in **Fig. 29**. The analytical results are very close to those issued from Fem.

The temperature distribution in the θ- and r-direction in the middle of the first cage rotor bar and the first stator slot is shown in **Figs. 30 ~ 31**. The accuracy of the new analytical model is established also in those subdomains where it is important to know the heat transfer for the insulation design. The effect of cooling outside the IM and inside the rotor shaft

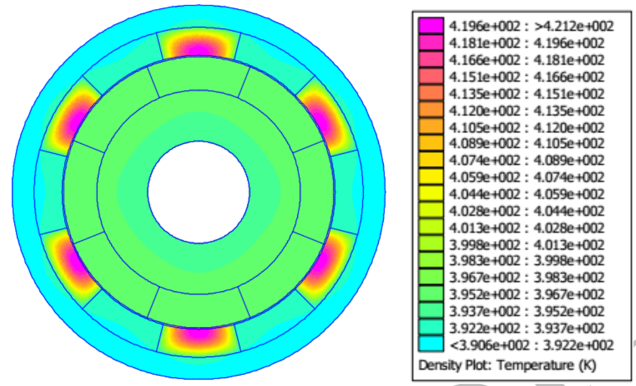

Fig. 28: Temperature distribution in the IM.

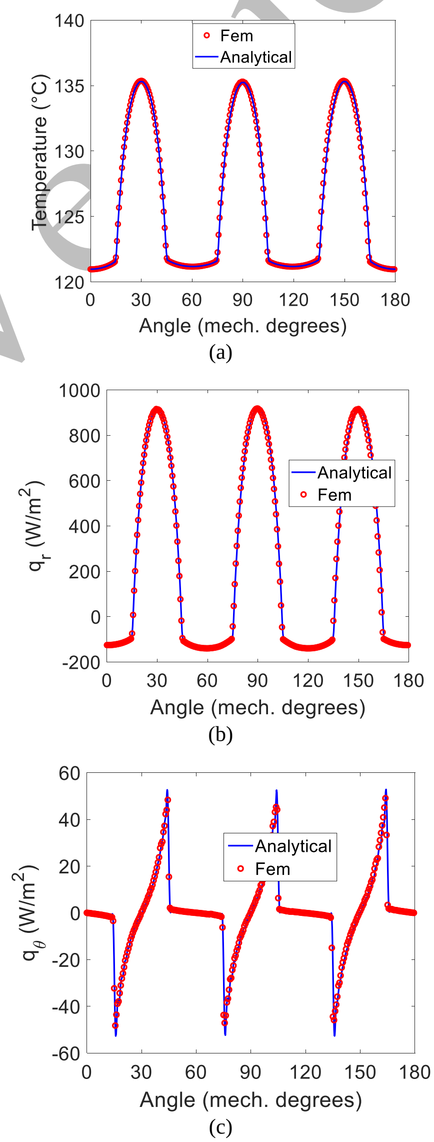

Fig. 29: Temperature and heat flux components distribution in the middle of air-gap.

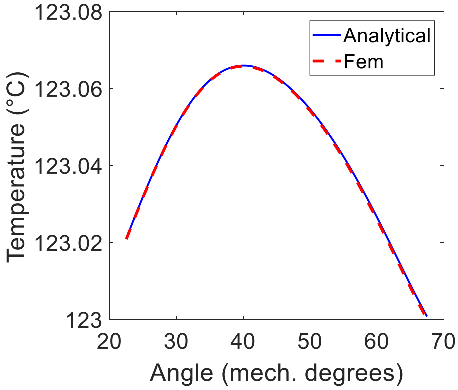

(a) In the θ-direction.

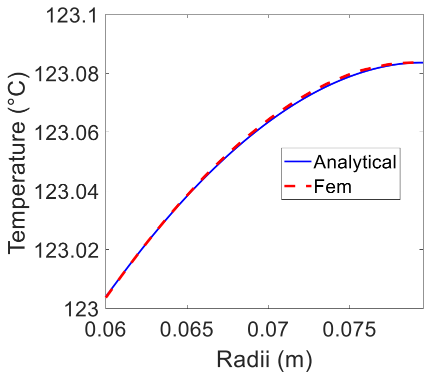

(b) In the r-direction.

Fig. 30: Temperature in the middle of the first cage bar.

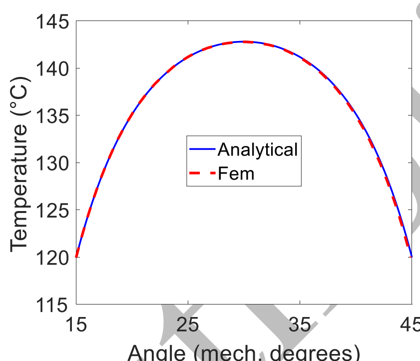

(a) In the θ-direction.

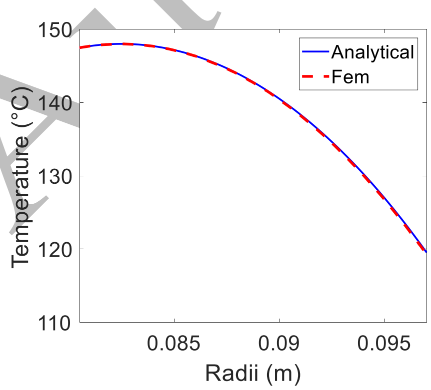

(b) In the r-direction.

Fig. 31: Temperature in the middle of the first stator slot.

is represented with the convective coefficients h_s and h_r respectively. For h_s equal to 20 W/(m^2 °K), which is small, we represent in **Figs. 32 ~ 33** the temperature distribution in the whole machine and in the middle of air-gap. The high temperature is located inside the stator and the temperature in the air-gap is higher also compared to h_s equal to 100 W/(m^2°K). For h_r equal to 20 W/(m^2°K) compared to h_r equal to 100 W/(m^2°K), the essential of heat is located in the rotor [see **Fig. 34**] and the temperature distribution in the air-gap [see **Fig. 35**] is higher than the case with h_r=100 W/(m^2°K). Low values of convective coefficients represent a barrier for heat transfer outside the stator and inside the rotor.

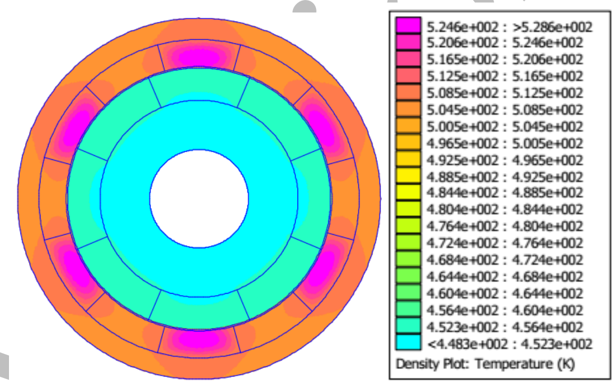

Fig. 32: Temperature distribution in the IM for h_s=20 W/(m^2 °K) and h_r=100 W/(m^2 °K).

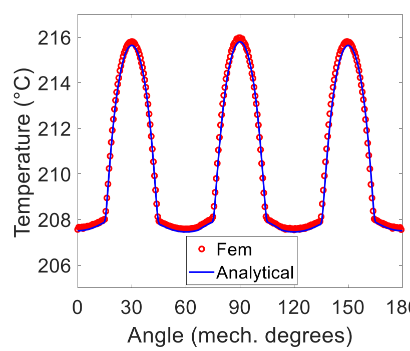

Fig. 33: Temperature distribution in the middle of air-gap for h_s=20 W/(m^2°K) and h_r=100 W/(m^2°K).

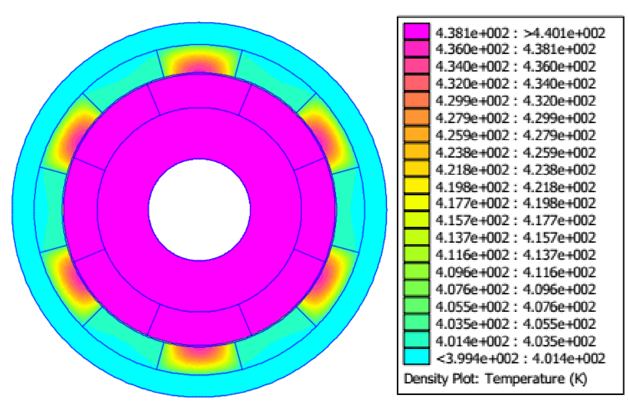

Fig. 34: Temperature distribution in the IM for h_r=20 W/(m^2°K) and h_s=100 W/(m^2°K).

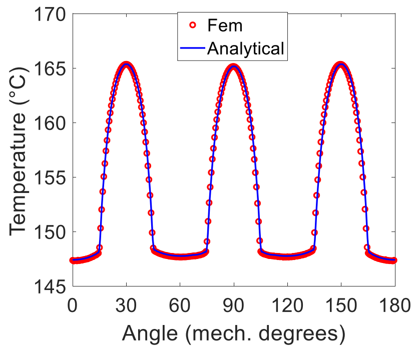

Fig. 35: Temperature distribution in the middle of air-gap for h_r=20 W/(m^2°K) and h_s=100 W/(m^2°K).

D. *Thermal Results of the Spoke Machine and Validation*

The exact analytical model for the Spoke machine has less number of regions and the rotor convective heat transfer in the rotor represent a BC of PMs and rotor teeth subdomains. The main dimensions and thermal parameters are given in **Tables I ~ II** with a difference in height and opening of PMs and rotor teeth. The heat sources used for the thermal model are the same as in the IPM. The analytical results are obtained with the number of harmonics for nn, mm, kk, $mm1$ and $kk1$ equal to 200, 70, 70, 60 and 60 respectively. The harmonics number is chosen to get accurate results with a reasonable time of calculation and to avoid numerical errors.

In **Fig. 36**, the temperature distribution in the machine obtained with Fem is shown. It can be observed that the temperature is higher in the slots due to Joule losses which are important in the slots. The temperature and heat flux components distribution in the middle of air-gap is represented in **Fig. 37**. The analytical results are very close to those obtained with Fem. To confirm the validity of the proposed analytical method for spoke-type machines, the temperature distribution in the center of the first PM and stator slot in both directions r and θ are shown in Figs. 38 and 39. In the PM and stator slots subdomains, the analytical results are also in very good agreement with those obtained with Fem.

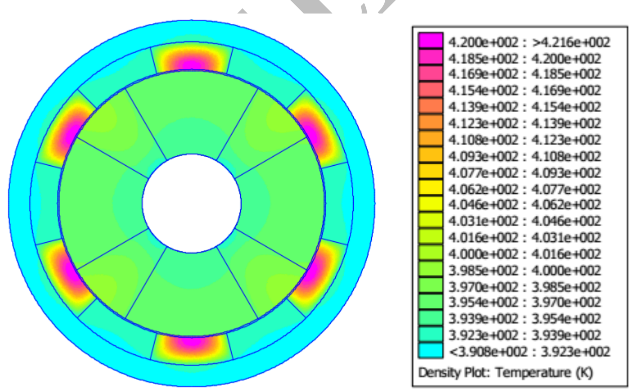

Fig. 36: Temperature distribution in the Spoke machine.

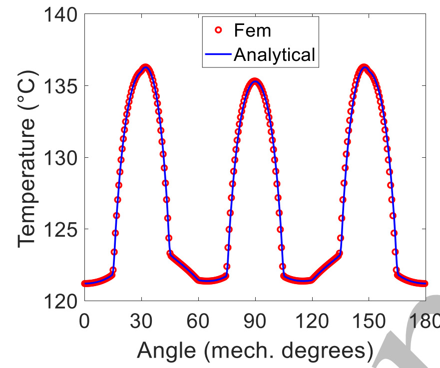

(a)

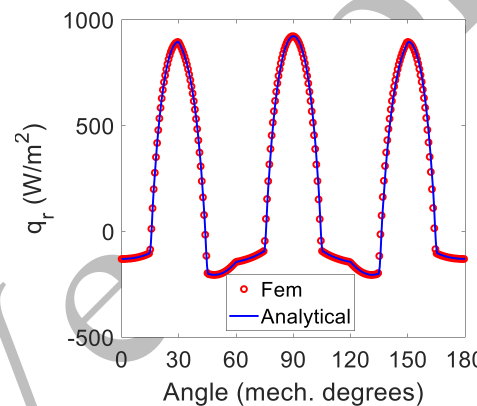

(b)

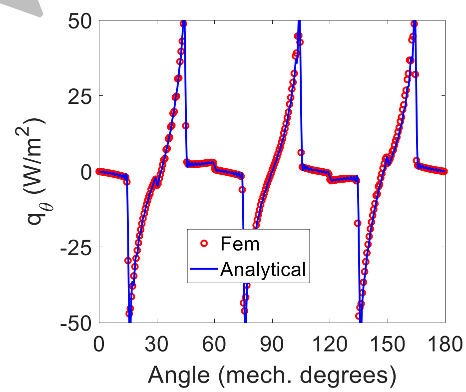

(c)

Fig. 37: Temperature and heat flux components distribution in the middle of air-gap.

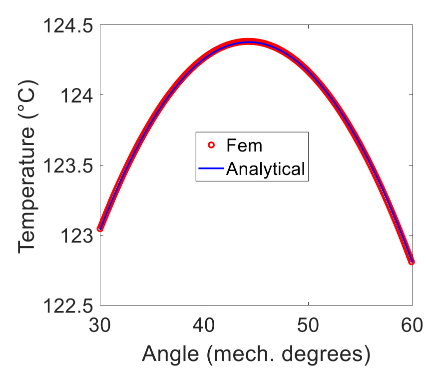

(a) In the θ-direction.

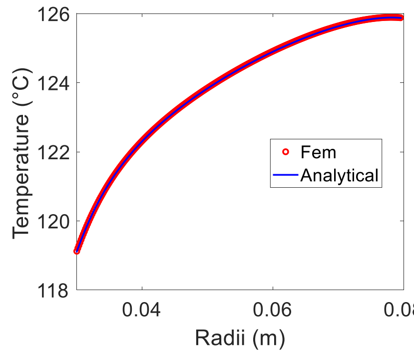

(b) In the *r*-direction.

Fig. 38: Temperature distribution in the middle of the first PM.

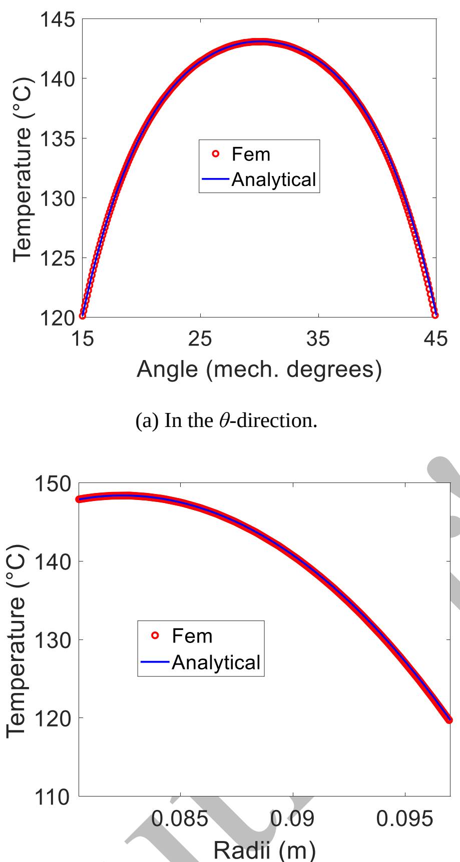

(a) In the θ-direction.

(b) In the *r*-direction.

Fig. 39: Temperature in the middle of the first stator slot.

IV. Conclusion

Actually, there is not 2-D exact analytical calculation of temperature and heat flux in electrical machines using formal resolution of heat equation. In this paper, we have proposed a new semi-analytical model based on the subdomain technique for prediction of steady-state temperature and heat flux components in four types of electrical machines. The model is valid for most rotating electrical machines and permits to determine the heat transfer in the entire machine with excellent accuracy. It can be used for a parametric study or an optimization process that include the effect of the variation of thermal conductivities, convective coefficients and power losses in temperature distribution. The analytical results are in very good agreement with those obtained by Fem.

Heat transfer using convection coefficient in the air-gap is also investigated and the results are very interesting.

References

[1] Sh. Utegenova, F. Dubas, M. Jamot, R. Glises, B. Truffart, D. Mariotto, P. Lagonotte, and Ph. Desevaux, "An Investigation Into the Coupling of Magnetic and Thermal Analysis for a Wound-Rotor Synchronous Machine," *IEEE Trans. Ind. Elect.*, vol. 65, no. 4, pp. 3406-3416, Apr. 2018.

[2] W. Jiang, and T.M. Jahns, "Development of Efficient Electromagnetic-Thermal Coupled Model of Electric Machines Based on Finite Element Analysis," *International Electric Machines and Drives Conference (IEMDC)*, pp. 816-823, 2013 (doi: 10.1109/IEMDC.2013.6556187).

[3] D. Geetha Nair, T. Jokinen, and A. Arkkio, "Coupled Analytical and 3D Numerical Thermal Analysis of a TEFC Induction Motor," *International Conference on Electrical Machines and Systems (ICEMS)*, pp. 103-108, 2015 (doi: 10.1109/ICEMS.2015.7385008).

[4] S. Nategh, O. Wallmark, M. Leksell, and S. Zhao, "Thermal Analysis of a PMaSRM Using Partial FEA and Lumped Parameter Modeling," *IEEE Trans. Energy Conv.*, vol. 27, no. 2, pp. 477-488, Jun. 2012.

[5] A.J. Grobler, S.R. Holm, and G. Van Schoor, "A Two-Dimensional Analytic Thermal Model for a High-Speed PMSM Magnet," *IEEE Trans. Ind. Elect.*, vol. 62, no. 11, pp. 6756-6764, Nov. 2015.

[6] G. Verez, H. Tiegna, G. Barakat, and G. Hoblos, "Analytical Thermal Modelling of Axial Flux Permanent Magnet Synchronous Machines," *International Conference on Electrical Machines (ICEM)*, pp. 2799-2805, 2012 (doi: 10.1109/ICElMach.2012.6350283).

[7] J. Nerg, M. Rilla, and J. Pyrhonen, "Thermal Analysis of Radial-Flux Electrical Machines With a High Power Density," *IEEE Trans. Ind. Elect.*, vol. 55, no. 10, pp. 3543-3554, Oct. 2008.

[8] A. Tüysüz, F. Meyer, M. Steichen, C. Zwyssig, and J.W. Kolar, "Advanced Cooling Methods for High-Speed Electrical Machines," *IEEE Trans. Ind. Appl.*, vol. 53, no. 3, pp. 2077-2087, Jun. 2017.

[9] L. Mo, X. Zhu, T. Zhang, L. Quan, Y. Wang, and J. Huang, "Temperature Rise Calculation of a Flux-Switching Permanent-Magnet Double-Rotor Machine Using Electromagnetic-Thermal Coupling Analysis," *IEEE Trans. Magn.*, vol. 54, no. 03, Mar. 2018, Art. ID 8201004.

[10] Z. Kolondzovski, A. Belahcen, and A. Arkkio, "Multiphysics thermal design of a high-speed permanent-magnet machine," *Applied Thermal Engineering*, vol. 29, no. 13, pp. 2693–2700, Sep. 2009.

[11] F. Li, P-Q. Ye, and H. Zhang, "Multi-physics analysis of permanent magnet tubular linear motors under severe volumetric and thermal constraints", *Journal of Central South University*, vol. 23, no. 7, pp. 1690-1699, Jul. 2016.

[12] K. Hruska, V. Kindl, and R. Pechanek, "Influence of temperature-dependent materials on mathematical modeling of thermal problems of induction machines," *European Conference on Power Electronics and Applications (EPE)*, pp. 1-8, 2013 (doi: 10.1109/EPE.2013.6631831).

[13] A. Boglietti, E. Carpaneto, M. Cossale, M. Popescu, D. Staton, and S. Vaschetto, "Equivalent Thermal Conductivity Determination of Winding Insulation System by Fast Experimental Approach," *International Electric Machines and Drives Conference (IEMDC)*, pp. 1215-1220, 2015 (doi: 10.1109/IEMDC.2015.7409216).

[14] S. Ouaged, M.A. Ben Hamida, Y. Amara, G. Barakat, and J.J.H. Paulides, "Thermal modelling of Tubular Linear Machines using a Hybrid Analytical Method," *International Conference on Sustainable Mobility Applications, Renewables and Technology (SMART)*, pp. 1-5, 2015 (doi: 10.1109/SMART.2015.7399242)

[15] H. Ennassiri, G. Barakat, and Y. Amara, "Steady state hybrid thermal modeling of permanent magnet electrical machines," *International Conference on Ecological Vehicles and Renewable Energies (EVER)*, pp. 1-6, 2016 (doi: 10.1109/EVER.2016.7476420).

[16] F. Dubas, and K. Boughrara, "New Scientific Contribution on the 2-D Subdomain Technique in Polar Coordinates: Taking into Account of

Iron Parts," *Math. Comput. Appl.*, vol. 22, no. 4, p. 42, Oct. 2017 (doi: 10.3390/mca22040042).

[17] L. Roubache, K. Boughrara, F. Dubas, and R. Ibtiouen, "New Subdomain Technique for Electromagnetic Performances Calculation in Radial-Flux Electrical Machines Considering Finite Soft-Magnetic Material Permeability," *IEEE Trans. Magn.*, vol. 54, no. 04, pp. 1-15, Apr. 2018, Art. ID 8103315.

[18] E. Devillers; J. Le Besnerais; T. Lubin; M. Hecquet, and J-P. Lecointe, "An Improved 2-D Subdomain Model of Squirrel-Cage Induction Machine Including Winding and Slotting Harmonics at Steady State," *IEEE Trans. Magn.*, vol. 54, no. 02, pp. 1-15, Feb. 2018, Art. ID 8100612.

[19] M. Pourahmadi-Nakhli, A. Rahideh, and M. Mardaneh, "Analytical 2-D Model of Slotted Brushless Machines With Cubic Spoke-Type Permanent Magnets," *IEEE Trans. Energy Conv.*, vol. 33, no. 1, pp. 373-382, Mar. 2018.

[20] B.L.J. Gysen, K.J. Meessen, J.J.H. Paulides, and E.A. Lomonova, "General Formulation of the Electromagnetic Field Distribution in Machines and Devices Using Fourier Analysis," *IEEE Trans. Magn.*, vol. 46, no. 01, pp. 39-52, Jan. 2010.

[21] K. Boughrara, N. Takorabet, R. Ibtiouen, O. Touhami, and F. Dubas, "Analytical Analysis of Cage Rotor Induction Motors in Healthy, Defective, and Broken Bars Conditions," *IEEE Trans. Magn.*, vol. 51, no. 2, Feb. 2015, Art. ID 8200317.

[22] D.C. Meeker. (Apr. 1, 2009). Finite Element Method Magnetics ver. 4.2. [Online]. Available: http://www.femm.info.

[23] M.L. Hosain, R. Bel Fdhila and K. Rönnberg, "Air-Gap Flow and Thermal Analysis of Rotating Machines using CFD," *Energy Procedia*, vol. 105, pp. 5153 – 5159, May 2017.

[24] D-D. Dang, X-T. Pham, P. Labbe, F. Torriano, J-F. Morissette, and C. Hudon, "CFD analysis of turbulent convective heat transfer in a hydro-generator rotor-stator system," *Applied Thermal Engineering*, vol. 130, pp. 17-28, Feb. 2018 (doi: https://doi.org/10.1016/j.applthermaleng.2017.11.034).

[25] X. Liu, H. Yu, Z. Shi, T. Xia, and M. Hu, "Electromagnetic-fluid-thermal field calculation and analysis of a permanent magnet linear motor," *Applied Thermal Engineering*, vol. 129, pp. 802-811, Jan. 2018 (doi: https://doi.org/ 10.1016/j.applthermaleng.2017.10.066).

[26] L. Roubache, K. Boughrara, F. Dubas, and R. Ibtiouen, "Elementary subdomain technique for magnetic field calculation in rotating electrical machines with local saturation effect," COMPEL, Under review, 2018.

[27] D.C. Meeker, "Rotating Losses in a Surface Mount Permanent Magnet Motor", October 2017, http://www.femm.info/wiki/SPMLoss.

Kamel Boughrara was born in Algiers, Algeria, in 1969. He received the Engineer Diploma from Ecole Nationale Polytechnique Algiers, Algeria, and the magister degree from the University of Sciences and Technology Houari Boumediene, Algiers, Algeria, in 1994 and 1997, respectively, and the Doctorat d'Etat degree from Ecole Nationale Polytechnique, Algeria, in 2008.

He is currently a Professor at Ecole Nationale Polytechnique (ENP), Algeria, and the Director of the Laboratoire de Recherche en Electrotechnique (LRE-ENP). His interests include modeling and control of electrical machines.

Frédéric Dubas was born in Vesoul, France, in 1978. He received the M.Sc. degree and the Ph.D. degree from the "Université of Franche-Comté" (Besançon, France) in 2002 and 2006, respectively, with a focus on the design and the optimization of high-speed surface-mounted permanent-magnet (PM) synchronous motor for the drive of a fuel cell air-compressor.

From 2014 to 2016, he has been the Head of "Unconventional Thermal and Electrical Machines" Team. He is the Head of the "Electrical Actuators" group in the "Hybrid & Fuel Cell Systems, Electrical Machines (SHARPAC)" Team. He works with ALSTOM Transports (Ornans, France), and RENAULT Technocenter (Guyancourt, France), where he is involved in the modelling, design and optimization of electrical systems and, in particular, induction and PM synchronous (radial and/or axial flux) machines, creative problem solving, and electrical propulsion/traction. He is currently an Associate Professor with the Département ENERGIE, FEMTO-ST Institute affiliated to the CNRS and jointly with the "Université of Franche-Comté" (Besançon, France).

He has authored over 100 refereed publications and he holds a patent about the manufacturing of axial-flux PM machines with flux-focusing. Dr. Dubas received the Prize Paper Awards in the IEEE Conference Vehicle Power and Propulsion (VPPC) in 2005 as well as the Prize Presentation Awards in the 19th International Conference on Electrical Machines and Systems (ICEMS) in 2017.

Rachid Ibtiouen received the Ph.D. degree in electrical engineering from Ecole Nationale Polytechnique (ENP), Algiers, Algeria, and the Institut National Polytechnique de Lorraine, Nancy, France, in 1993.

He was with the Groupe de Recherche en Électrotechnique et Électronique de Nancy, Nancy, from 1988 to 1993. From 1993 to 2011, he was an Expert Member of the Committee of Evaluation of the University Projects of Research with the Comité National d'Evaluation et de Programmation de la Recherche Universitaire (CNEPRU), Ministry of the Algerian Higher Education. From 2005 to 2013, he was the Director of the Laboratoire de Recherche en Electrotechnique with ENP (LRE-ENP). He is currently a Professor and the Associate Director of Research with ENP. He is also the Head of the Department of Electrical Engineering with ENP. His current research interests include the modeling of electric systems and drives, and, in particular, electrical machines.